Volume 2 | Number 12 | December 2015

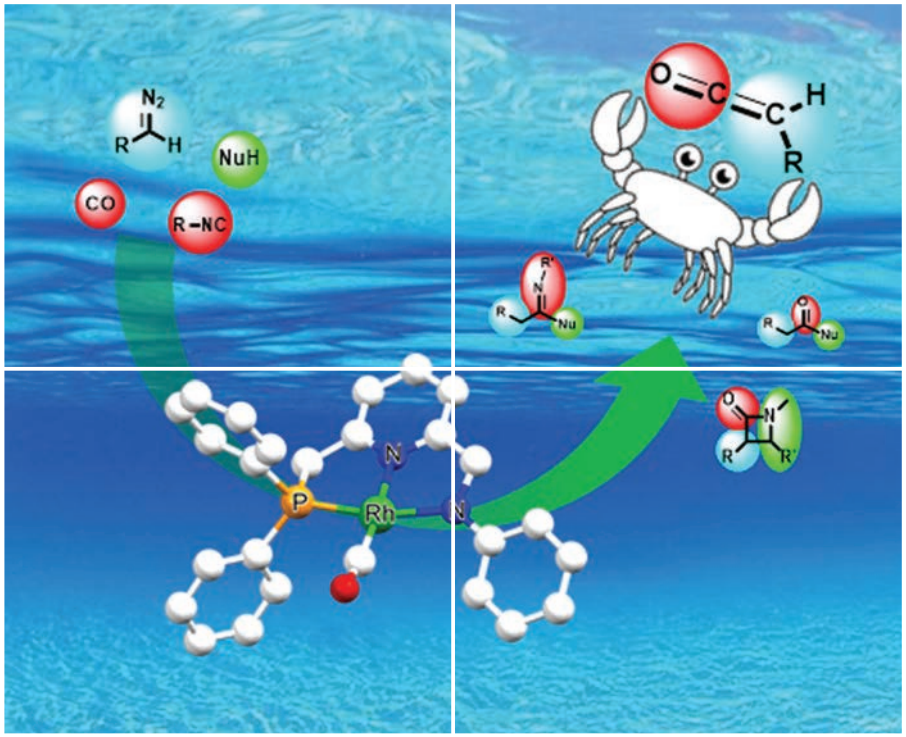

ORGANIC CHEMISTRY

FRONTIERS

Chinese Chemical Society
SIOC 1950
ROYAL SOCIETY OF CHEMISTRY
http://rsc.li/frontiers-organic

ORGANIC CHEMISTRY
FRONTIERS

RESEARCH ARTICLE

View Article Online
View Journal | View Issue

Cite this: *Org. Chem. Front.*, 2015, **2**, 1561

Rhodium catalysed conversion of carbenes into ketenes and ketene imines using PNN pincer complexes†

Z. Tang,[a] S. Mandal,[a] N. D. Paul,[a] M. Lutz,[b] P. Li,[a] J. I. van der Vlugt[a] and B. de Bruin*[a]

Ketene synthesis involving catalytic carbonylation of carbenes is an interesting alternative to traditional synthetic protocols, offering milder conditions to diversified products. Analogous catalytic ketene imine production from carbenes and isocyanides is also a promising reaction. However, both methods are underdeveloped. Rhodium carbonyl complexes **B** and **E**, based on (6-(phosphinomethyl)pyridin-2-yl)-methan-*sec*-amine type PNN ligand scaffolds, reveal good catalytic activities in ketene and ketene imine production using ethyl diazoacetate (EDA, **1**) or sodium 2-benzylidene-1-tosylhydrazin-1-ide (**5**) as the carbene precursors, as demonstrated by *in situ* amide/imidamide and β-lactam synthesis. DFT calculations suggest that diazo activation is the rate-determining step and that N*H*-deprotonation of the ligand produces a more active rhodium complex. The ketene formation step likely proceeds *via* an outer-sphere CO insertion mechanism. Subsequent stepwise and concerted [2 + 2] cyclization mechanisms have comparable barriers. The complexes are the first rhodium catalysts reported for catalytic ketene/ketene imine production from carbenoids. The higher affinity of rhodium for binding ketene or ketene imine intermediates as compared to other reported metal catalysts (*i.e.* Pd, Co) may provide opportunities for future enantioselective reactions when using chiral ligands.

Received 16th September 2015,
Accepted 15th October 2015

DOI: 10.1039/c5qo00287g

rsc.li/frontiers-organic

Introduction

Ketenes[1] are highly reactive and useful intermediates to a wide range of important chemicals for pharmaceuticals and fine chemicals, such as esters, amides, β-lactons or β-lactams.[2] Ketene imines, the isoelectronic nitrogen analogues, are also reactive and versatile intermediates that tend to undergo analogous coupling reactions to give relevant nitrogen-containing compounds.[2b,3]

Ketenes are conventionally synthesized by thermolysis,[4] Wolff rearrangement[5] or dehydrohalogenation of acyl halide precursors.[6] These methods generally have limitations, such as a narrow substrate scope, strictly controlled conditions and generation of detrimental side products. Ketene imines are generally synthesized from ketenes *via* an aza-Wittig reaction,[7] various rearrangement reactions[8] or azide–alkyne coupling.[9] These methods have similar limitations concerning the substrate scope and reaction conditions.

Ketene chemistry has a close connection with carbenes.[10] Carbonylation of carbenes to give ketene formation was reported in 1912,[11] and the reactivity to undergo carbonylation has remained a characteristic feature of carbenes. A number of early or late transition metal complexes have been reported to mediate carbonylation of carbenes to form ketenes.[10,12] This strategy to construct ketenes should allow a larger substrate scope, as a wide variety of diazo-compounds and their precursors are easily accessible. Possibly, also milder reaction conditions should be achievable. However, most reported reactions are strictly stoichiometric and usually require a high CO pressure and/or high reaction temperatures.

The catalytic version of ketene synthesis from carbonylation of carbenes has been largely underdeveloped,[13,14] with cobalt[14b,d,f] and palladium[14e] catalysts being reported only very recently. Ketenes were generated with these catalysts in decent yields under relatively mild conditions (1–20 bar of CO, 50–60 °C), and *in situ* converted for the synthesis of a range of esters, amides and β-lactams (Scheme 1), using diazo[14] and *N*-tosylhydrazone[15] compounds as carbene precursors.

Although stereocontrol in the coupling reactions of ketene is highly desirable,[1,16] the transition metal catalysts reported thus far for ketene formation from carbene precursors are not

[a]*Supramolecular, Homogeneous & Bio-inspired Catalysis, van't Hoff Institute for Molecular Sciences, University of Amsterdam, Science Park 904, The Netherlands. E-mail: b.debruin@uva.nl*
[b]*Crystal and Structural Chemistry, Bijvoet Center for Biomolecular Research, Utrecht University, Padualaan 8, 3584 CH Utrecht, The Netherlands*

† Electronic supplementary information (ESI) available. CCDC 1424620, 1423805 and 1423806. For ESI and crystallographic data in CIF or other electronic format see DOI: 10.1039/c5qo00287g

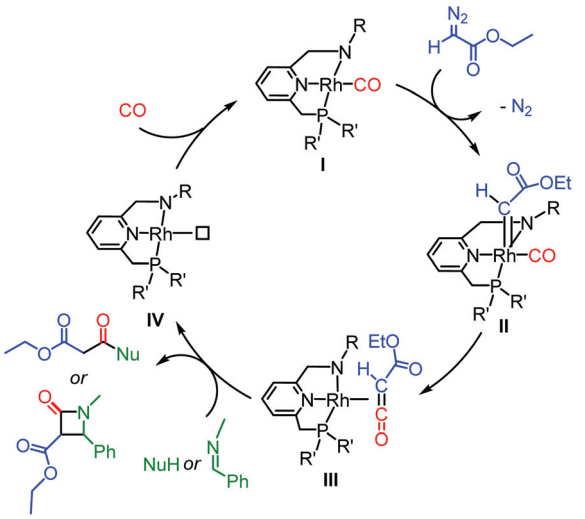

Scheme 1 The envisioned catalytic cycle of ketene formation and subsequent coupling reaction mediated by Rh PNN complexes (only inner-sphere CO insertion pathway depicted).

able to promote the follow-up coupling reactions in an enantioselective or diastereoselective manner (*e.g.* when several chiral Co(porphyrin) complexes were used as catalysts, no ee was detected[14f]). This is attributed to a low affinity of the metal ions to bind the ketene intermediate, which as a result undergoes coupling reactions after its release from the metal centre.

A single molecular catalyst that can catalyse ketene formation from carbenes and can induce stereoselectivity in the coupling reactions would be highly desirable. Our consideration on catalyst development for this purpose was to utilize the Rh(PNN) scaffold developed earlier in our lab, as rhodium has been recognized as one of the most active metals to mediate the carbonylation of carbenes to form ketenes,[10a] and rhodium should have a relatively high affinity to bind the ketene intermediates, of key-importance for future chirality transfer. In addition, the PNN ligand is a versatile scaffold with both the amine and the phosphine available to install chiral auxiliaries in future studies. The rigidity of the pincer ligand is also expected to provide stability to the metal complex during the reaction. Furthermore, derivatives of the complexes upon –NH deprotonation are accessible, offering easy modification and diversity in the number of complexes to screen for catalytic activity. While the studies in this report focus on achiral model systems, the results are nonetheless relevant for future development of enantioselective catalysis.

In the envisioned catalytic working model, the diazo compound (ethyl diazoacetate, EDA, is taken as an example in Scheme 1) first coordinates to Rh complex **I** before being converted to the metallocarbene intermediate **II** *via* N_2 loss. Subsequent CO insertion into the metallocarbene (*via* either an inner- or outer-sphere mechanism; the inner-sphere mechanism being shown in Scheme 1) then results in formation of the metal-ketene species **III**. Follow-up reactions, such as nucleophilic coupling or [2 + 2] imine-ketene cyclization, can occur in the coordination sphere of the metal. If the PNN ligand bears chiral substituents, enantioselective coupling may be envisioned. After the coupling, release of the product and (possible) coordination of exogenous CO would close the catalytic cycle. Ketene imines can be prepared in a similar manner by using isocyanides in place of CO.[3] Examples of the stoichiometric reaction are not abundant,[17] but examples of catalytic synthesis of ketene imines are even scarcer and limited to only two recently reported palladium catalysts.[18] We therefore considered it worthwhile to develop a protocol for catalytic metal-mediated ketene imine synthesis, and these studies are included herein.

The main goals of the investigations presented here are: (I) To show that Rh(PNN) complexes are viable carbene-transfer catalysts for ketene and ketene imine synthesis, and (II) to investigate computationally whether the overall catalytic reaction could proceed *via* rhodium-coordinated ketenoid intermediates that undergo attack by external nucleophiles in the coordination sphere of rhodium (the latter being obviously relevant for future development of enantioselective strategies with chiral analogs of the complexes studied herein).

Results and discussion

Synthesis of the PNN ligands

The PNN ligands **a** and **b**, with phenyl substituents at phosphorus, were synthesized *via* pathway [1] (Scheme 2), a modifi-

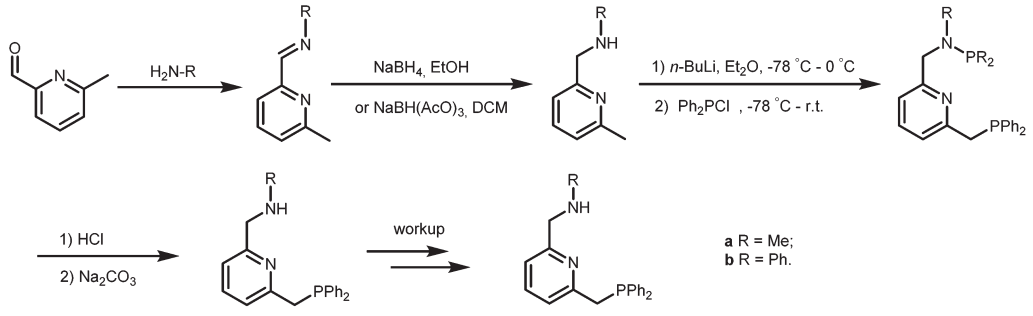

Scheme 2 Synthetic pathway [1] for the synthesis of ligands **a** and **b**.

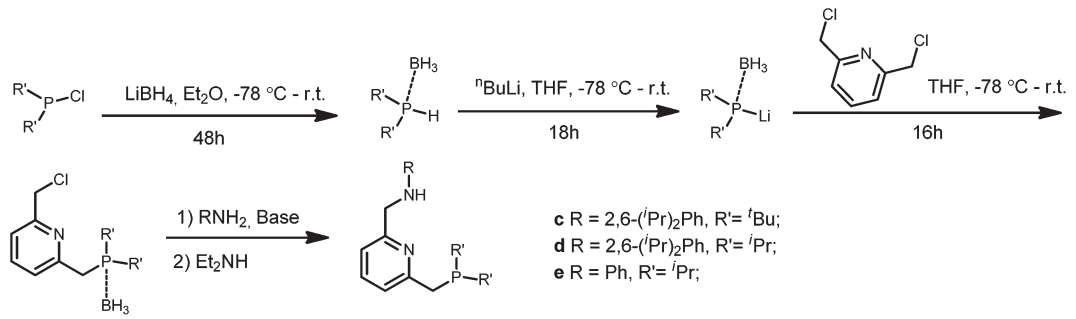

Scheme 3 Synthetic pathway [2] for the synthesis of ligands **c–e**.

cation from a previously reported procedure.[19] Synthesis of **a** and **b** starts with condensation of 6-methylpicolinaldehyde with the desired amines, followed by imine reduction to the amines. The isolated amines were treated with two equivalents of *n*-butyl lithium (^{n}BuLi) in diethyl ether (Et_2O) at −78 °C, with subsequent cannulation of this reaction mixture to a solution of Ph_2PCl in Et_2O at −78 °C and acidic work-up to afford the PNN ligands **a** and **b** in 15–20% overall yields.

The PNN ligands **c–e**, which bear alkyl substituents at phosphorus, were synthesized *via* pathway [2] (Scheme 3), also following a modified literature procedure.[20] Borane was used as protecting group for the alkylphosphine intermediates to allow purification processes to be performed under aerobic conditions. Subsequent installation of the phosphine arm and the nitrogen arm on 2,6-bis(chloromethyl)pyridine followed by borane removal afforded the pincer ligands **c**, **d** and **e** in 34–44% overall yields.

Synthesis of the PNN rhodium carbonyl complexes

The targeted Rh(CO)(PNN) complexes were obtained by reaction of $\{[Rh(CO)_2(\mu\text{-}Cl]_2\}$ with two equivalents of the respective PNN ligands in methanol, followed by salt metathesis using NH_4PF_6 (Scheme 4).[21] Five complexes were synthesized and isolated. Complexes **A** and **B** both have a phenyl-substituted phosphine arm, only differing in the substituent on the nitrogen arm (methyl for **A** and phenyl for **B**). Complexes **C** and **D** both have bulky 2,6-isopropylphenyl substituents on the nitrogen arm. They differ in the substituents at phosphorus atom (isopropyl for **C** and *tert*-butyl for **D**). Complex **E** is an analogue of complex **D** with a phenyl substituent on the nitrogen arm. Deprotonation of the amine moieties of cationic complexes **B–E** produces the neutral amido complexes **B′–E′** (Scheme 4),[22] but these were not isolated.

Yellow single crystals of complex **A** were obtained by storing a concentrated methanol solution of **A** at 0 °C, while crystalline material for **B** and **E** was obtained by top-layering the corresponding concentrated dichloromethane (DCM) solution with diethyl ether (Et_2O). The X-ray crystal structures[23] of the three complexes are depicted in Fig. 1, and selected bond lengths and angles are listed in Table 1. All the three complexes adopt a slightly distorted square planar geometry around Rh, with the plane defined by the atoms P1, N1 and N2. Bond lengths and angles around Rh in these complexes are similar.

Slightly longer Rh–N2 bonds in **B** and **E** than in **A** (2.1609 and 2.1626(13) *vs.* 2.1381(10) Å) reflect a slightly weaker donor capacity of the N2 donor in complexes **B** and **E**. The infrared spectra in CD_2Cl_2 solution show a higher CO stretching frequency in **B** than in **A** (2007 *vs.* 2002 cm^{-1}) is in agreement with weaker metal-to-carbonyl back-donation in **B**. Lower CO stretching frequencies in complexes **C**, **D** and **E** were observed (1999, 1996 and 1999 cm^{-1}, respectively), as these ligands bear more electron-rich alkylphosphine ligands.

Catalytic results

Amide synthesis *via* catalytic ketene formation using EDA as the carbene precursor. The complexes **A–E**[22] have been tested

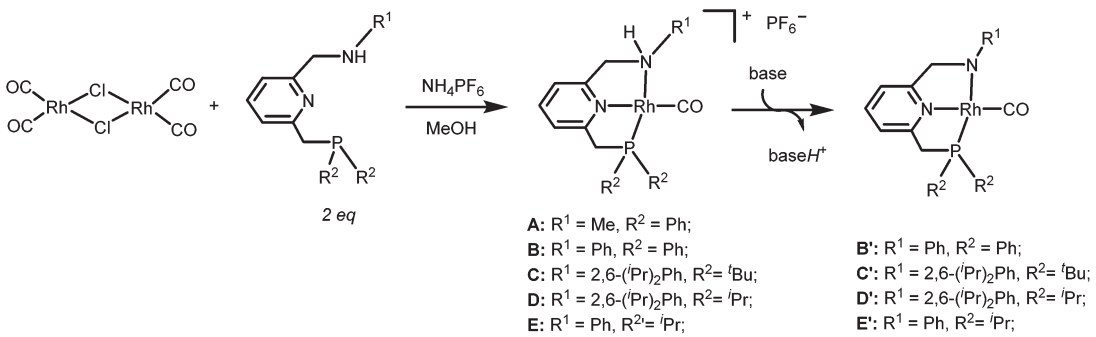

Scheme 4 Synthesis of cationic amine Rh(CO)(PNN) complexes **A–E** and their neutral amido analogues **A′–E′**.

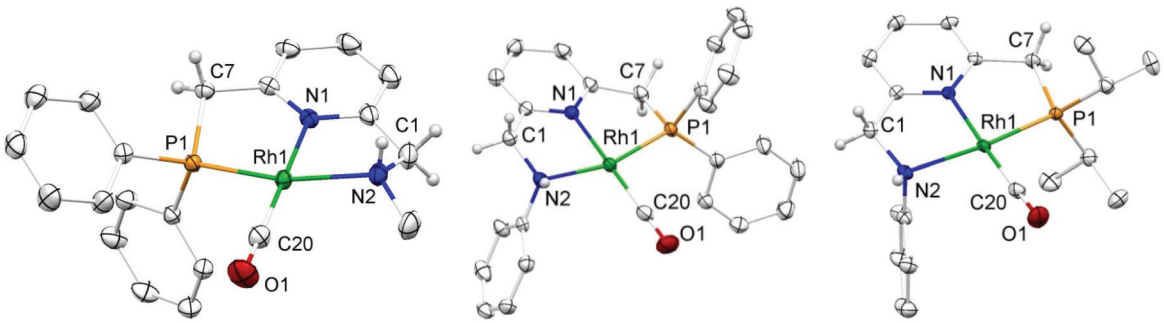

Fig. 1 Molecular structures (ORTEP at 50% level) of the cationic complexes **A** (left), **B** (middle) and **E** (right). Counter ions and hydrogen atoms are removed for clarity, except for those on C1, C7 and N2. In **A**, only the major disorder form of the coordinated amine group is shown.

Table 1 Selected bond lengths (Å) and angles (°) for complex **A**,[23] **B** and **E**

	A	**B**	**E**
Rh1–P1	2.2234(3)	2.2120(9)	2.2126(4)
Rh1–N1	2.0540(9)	2.053(3)	2.0483(12)
Rh1–N2	2.1381(10)	2.160(3)	2.1624(13)
Rh1–C20	1.8283(12)	1.831(4)	1.8383(16)
C20–O1	1.1489(15)	1.147(5)	1.139(2)
P1–Rh1–N1	82.83(2)	83.59(8)	84.77(3)
P1–Rh1–N2	161.78(3)	163.53(9)	161.18(4)
N1–Rh1–C20	176.57(4)	175.19(15)	176.44(6)
Rh1–C20–O1	178.01(12)	176.0(4)	178.64(17)

as catalyst precursors for catalytic ketene formation by carbonylation of carbenes (Table 2). Ethyl diazoacetate (EDA) was used as the carbene precursor, with toluene as the solvent at 60 °C under 20 bar of CO, and 4-nitro-aniline **2a** was used as the nucleophile to trap the ketene intermediate. The reaction typically produced mixtures containing ethyl 3-((4-nitrophenyl)-amino)-3-oxopropanoate (**3a**) and ethyl (4-nitrophenyl)glycinate (**4**) (see Table 2), with **3a** being the desired product resulting from the ketene intermediate **III** and **4** being an undesired side product from the direct reaction between 4-nitro-aniline **2a** and carbene intermediate **II** (see also Scheme 1, for labeling of the intermediates **II** and **III**).

Table 2 Amide synthesis *via in situ* generated ketene with EDA as the carbene precursor

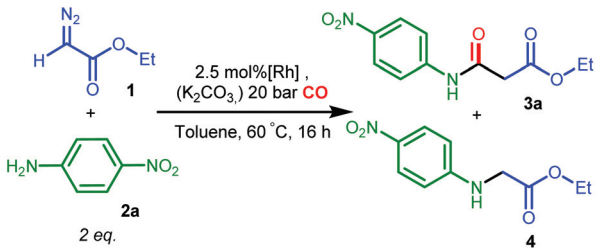

Entry	Catalyst	2 eq. K_2CO_3	**3a** + **4** yield (%)	**3a**/**4** ratio	Remarks
1	**A**	×	50	0.4	
2	**A**	√	26	0.2	
3	**B**	×	100	0.4	38 h
4	**B**	√	100	7.4	38 h
5	**B**	√	94	9.7	
6	**C**	√	12	0.6	
7	**D**	√	14	0.4	
8	**E**	√	100	>50	

For complex **A**, poor selectivities with moderate or low yields to the desired amide product **3a** were obtained, either in the absence or presence of K_2CO_3 (entries 1 and 2, Table 2). In contrast, the diphenylphosphine complex **B** with phenyl substituents on the amine nitrogen gave much better results in the presence of the base, both in terms of yield and selectivity to **3a** (entries 4, 5, the small selectivity difference might originate from overlap of signals used for integration in the ^{1}H NMR spectra), while amine **4** was obtained as the major product in the absence of the base.

The nucleophilic coupling with the ketene appears to be accelerated to a larger extent than the side reaction under these basic conditions. This suggests that amine deprotonation of **B** to form the neutral amido complex **B′** (see Scheme 4) is beneficial for the selectivity.

One might hypothesize that for the neutral amido complex **B′** the carbene intermediate **II** is less prone to external attack by the aniline **2a**, due to increased π-back donation to the carbene p-orbital (as a result of increased electron density) as compared to the cationic amine complex **B**, whereas CO migration or external CO attack to the carbene moiety to form the ketene might be facilitated by the increased nucleophilicity of the carbene ligand (taking advantage of the electron-accepting properties of CO). Control experiments showed that complex **A** was inert toward deprotonation by K_2CO_3, while **B** was readily deprotonated by K_2CO_3 in THF,[24] consistent with the assumption that a neutral amido intermediate is the active species.

The poor performance of complexes **C** and **D** is probably related to steric shielding by the bulky side-groups in these ligands, while the less bulky complex **E** (in its deprotonated form **E′**) gave almost full conversion and a very high selectivity (**3a**/**4** ratio >50) to **3a** (entry 8) in 16 hours. Deprotonated complex **E′** clearly outperforms all other catalysts screened in

this study, both in terms of activity and selectivity. Complexes **B′** and (in particular) **E′** are thus determined to be supreme catalysts for ketene generation with EDA as the substrate.

Sodium *N*-tosyl hydrazone salt 5 as the carbene precursor. Interestingly, the product selectivity with respect to ketene formation *versus* direct attack of the carbenoid intermediate by the aniline substrate not only depends on the applied catalyst, but also on the carbene precursor used. With carbene precursor **5** (see Scheme 5) the selectivity of catalyst **B′** can actually exceed that of **E′**. When using *N*-tosylhydrazone salt **5** (sodium 2-benzylidene-1-tosylhydrazin-1-ide), a precursor of (diazomethyl)benzene, different catalytic activities and selectivities for the formation of amide product **6a** were obtained, affording both a higher yield and selectivity with complex **B′** as compared to **E′**. Interestingly, for these reactions an *imine* side product **7a** was obtained instead of an *amine* product (Table 2). Formation of this imine side product **7a** was confirmed by mass spectrometry and ^{1}H NMR spectroscopy. This compound could well be formed in a condensation reaction of **2a** with benzaldehyde, which could be formed by oxidation of the diazo intermediate, *trans*-imination between **2a** and the corresponding hydrazone of **5**,[25] or hydrolysis of the latter.[26] Surprisingly, the use of different batches of substrate **5** led to differences in the yields obtained. For some batches of **5** (denoted as "batches 1" in the ESI†) rather high yields were obtained at mild reaction temperatures, while for other batches of **5** (denoted as "batches 2" in the ESI†) only poor yields (generally <35%) were obtained under similar conditions (*i.e.* runs at 55 °C for 20 hours). In the latter case significant amounts of the starting compound **5** were detected in the reaction mixture by ^{1}H NMR spectroscopy, thus indicating that slow conversion of **5** to the required diazo species was the problem. The slow thermolysis of some batches of **5** as compared to others at low temperatures (*i.e.* 55 °C) is most likely related to morphology differences between the different batches of this poorly soluble solid material. For the less reactive batches, a reaction temperature of 80 °C was required to obtain moderate yields of the desired products (see ESI, Table S1†).

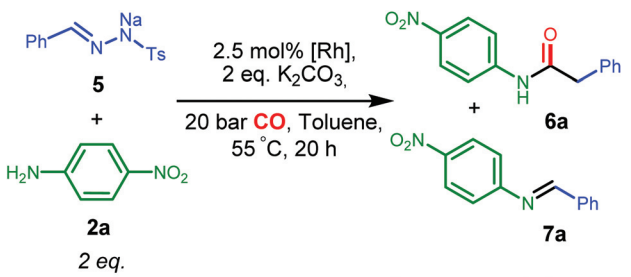

[Rh]	6a+7a Yield (%)	6a/7a ratio
B	63	9.1
E	58	6.7

Scheme 5 Catalytic activities of complexes **B** and **E** for synthesis of amide **6a** from **5** and **2a**.

β-Lactam synthesis *via* catalytic ketene formation

β-Lactams are medicinally important structures and versatile building blocks for other valuable compounds.[27] A number of methods are available to synthesize these compounds, with [2 + 2] Staudinger ketene-imine cyclization being among the most extensively used and studied protocols.[28] Recently, novel synthetic protocols were developed that enhance the synthetic applicability of Staudinger-type β-lactam synthesis, making use of *in situ* generated ketenes *via* catalytic carbonylation of diazo-derived carbenes in one-pot synthetic protocols to prepare the respective β-lactams.[14] This was shown to be a useful alternative to more traditional β-lactam synthesis. The next step in this field is to develop enantioselective versions of these reactions. However, this is not so trivial, as the ketene intermediates seem to have low affinity for the catalysts applied thus far. Hence we studied the Rh(PNN) complexes as catalysts for this reaction.

Using similar conditions as the recently reported literature,[14e,f] we tested the catalytic activity of the complexes in the reaction using *N*-benzylidenemethanamine **8a** as the imine substrate.

Surprisingly, when EDA was used as the substrate, the complexes **B** or **E**, identified as supreme catalysts in catalytic ketene synthesis for amide formation, gave generally no formation or less than 5% yield to the expected β-lactam product, either in the presence or absence of K_2CO_3, with no identifiable side products and in many cases unreacted EDA detected after the reaction. The exact reason behind this behaviour is not clear, as EDA can be used in catalytic ketene formation as demonstrated by the reactions described in Table 2. Nonetheless, EDA and imine **8a** are poor coupling partners in catalytic formation of β-lactams when using catalyst **B** or **E**. The Rh complexes tested are thus not compatible with the carbene precursor EDA for the corresponding β-lactam synthesis under the currently applied conditions.

In marked contrast to the results obtained with EDA, using the *N*-tosylhydrazone salt **5** as the carbene precursor led to more selective reactions, producing the β-lactam product **9a** (Table 3). In the series of complexes **A–C** and **E**, complex **B** gave the highest yield of the desired β-lactam product **9a** (67.7%), while **E** (which was one of the best performing catalysts for the reactions described in Table 2) gave only a moderate yield of 33.0%. Complex **A** gave no formation of β-lactam, while complex **C** led to low yield and 23.1% of the (free) phenyl ketene, according to ^{1}H NMR spectroscopy. It should be noted that **5** is also a relative strong base, hence the corresponding Rh complexes are expected to exist in their N*H*-deprotonated neutral amido forms in the catalytic reaction, even in the absence of additional base. In all cases, the *trans*-configured β-lactam was the predominant isomer, while the *cis*-isomer was either not detected or present as a minor product (assignments based on literature[14e]). The *trans–cis* stereoselectivity has been a poorly understood and controversial topic in the Staudinger reaction.[29] Previous studies have shown that the stereoselectivity may be related to isomeriza-

Table 3 Rhodium catalyst screening for β-lactam **9a** synthesis from **5** and **8a**

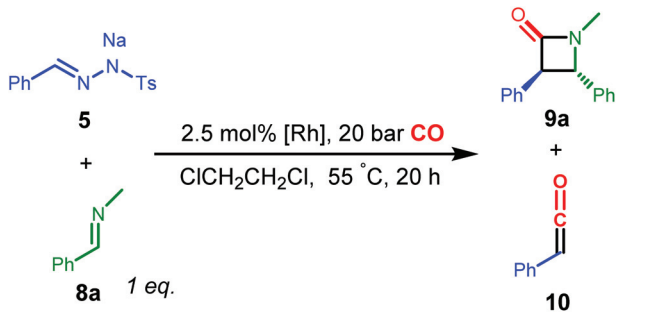

Entry	Catalyst	Yield of **9a** (%)	Yield of **10** (%)
1	**A**	0	
2	**B**	67.7	
3	**C**	7.2	23.1
4	**E**	33.0	

tion of the imine or zwitterionic intermediate, and is determined by many factors such as solvent and temperature, but most importantly the substituents of both the ketene and the imine. As higher *trans*/*cis* ratios of the product **9a** were generally observed with the rhodium catalyst system than for non-catalysed systems[29c] and those with Pd[14e] and Co[14f] systems under similar or identical conditions, we believe that the cyclization process is also metal-catalysed.[30] Metal-involvement in the [2 + 2] ketene-imine cyclization has been suggested for ketenes generated from carbonylation of Fischer carbenes.[31] As such, this is a promising observation, stimulating further research in the development of enantioselective reactions.

Variation of the *para*-substituent on the phenyl ring of imine **8** has an effect on the yield of products **9**, but in all cases moderate to excellent activities for coupling with the *in situ* generated ketene were observed (see ESI, Table S2†).

Catalytic ketene imine synthesis from carbene precursor 5 and *tert*-butyl isocyanide 11

Ketene imines, the nitrogen analogues of ketenes (*e.g.* **12** in Scheme 6), represent an important class of reactive species and useful synthetic intermediates, which are able to undergo nucleophilic coupling or cyclization reactions for the production of various pharmaceutically valuable molecules, *e.g.* substituted isoquinolines and pyridines.[2b,3] As the rhodium complex **B** showed good catalytic activities in mediating ketene formation *via* carbonylation of carbenes, we were interested to extend the synthetic concept to catalytic ketene imine synthesis from carbenes and isocyanides, which are isoelectronic to CO. As this reaction has thus far mostly been studied stoichiometrically,[17] development of catalytic methods should be practically useful,[18] potentially allowing a wide substrate scope and an alternative mild condition route to traditional ketene imine synthesis.

While EDA turned out to be an unsuitable carbene precursor for the reaction (no ketene imine was observed after a series of reaction optimizations with and without K_2CO_3), the hydrazone salt **5** in combination with *tert*-butyl isocyanide **11** gave 50.7% yield of the phenyl ketene imine **12**, catalysed by complex **B** at 55 °C overnight (see ESI, Table S3†). Excess **11** is beneficial, producing ketene imine **12** in a higher yield (entries 1 and 2, Table S3†). To the best of our knowledge, this is the first example of catalytic synthesis of any ketene imine from a carbene precursor and an isocyanide. Different batches of **5** again led to irreproducibility of yields and a need to use a higher reaction temperature to covert certain batches of tosyl hydrazone salt **5** to the diazo compound (see Table S3†).

We next investigated the one-pot synthesis of 2-phenylacetimidamide **13** by adding an amine nucleophile **2b** to the *in situ* generated ketene imine (Scheme 6), which led to 30.0% yield of the desired product **13** along with 64.3% of the intermediate ketene imine **12**, despite a reaction time of 44 hours. This possibly relates to the lower electrophilicity of ketene

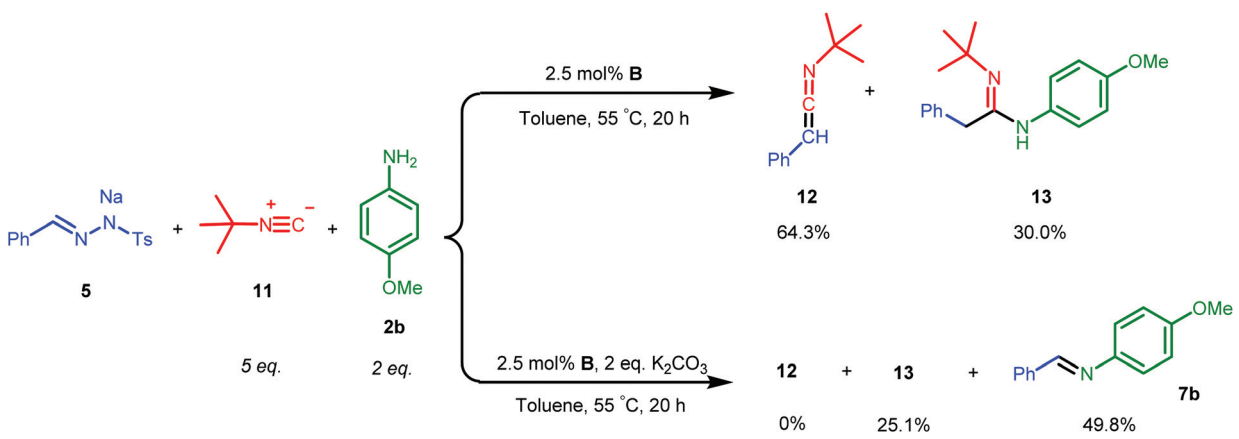

Scheme 6 Acetimidamide **13** synthesized by one-pot catalytic ketene imine formation from **5** and **11** and subsequent trapping of ketene imine **12** by aniline **2b**.

imines as compared to ketenes, or (perhaps more likely) serves as an indication that the coupling reaction is also catalysed by the metal complex, which is possibly slowed down by catalyst deactivation over the course of the reaction. Addition of two equivalents of K_2CO_3 was expected to accelerate the coupling process. However, while the ketene imine **12** was not observed after 18 hours, the 2-phenylacetimidamide **13** was obtained only in 25.1% yield, and the imine product **7b** was obtained as the major product in 49.8% yield. Further optimizations by varying the base, solvent and ratio of agents could result in selectivity improvements, but this was not attempted because it appears right now that the Rh(PNN) systems are too sensitive to allow high conversions of **12** to **13** in one-pot transformations using the same catalyst.

Mechanistic studies

DFT calculations on ketene formation and β-lactam formation. DFT-D3 calculations at the BP86/def2-TZVP level were performed in order to examine the possible mechanisms of catalytic ketene formation, as well as the follow-up ring-closure steps between the ketene intermediate and the imine substrate. One of the main questions regarding the mechanism of the Rh-catalysed β-lactam formation is whether the overall process involves catalytic ketene formation followed by un-catalysed coupling of the imine with the free ketene, or whether the imine-ketene coupling step is also Rh-catalysed proceeding *via* a rhodium-coordinated ketene moiety. This is important to assess the feasibility of developing any enantioselective protocols. Another important question we tried to answer with DFT is whether ketene formation by carbonylation of the metallocarbene intermediate involves the carbonyl ligand that is already coordinated to rhodium as a ligand (inner-sphere mechanism) or proceeds *via* external CO attack at the carbenoid intermediate (outer sphere mechanism). The ketene-imine [2 + 2] cyclization step can also differ with respect to whether the imine coordinates to the metal centre prior to reaction or not. Hence, several possible pathways were studied with DFT methods: A completely inner-sphere pathway $\mathbf{P_{II}}$ with both ketene formation and ring-closure of the ketene with the imine proceeding *via* internal attack; A completely outer-sphere pathway $\mathbf{P_{OO}}$, with both steps involving external attack of substrates to coordinated carbene and ketene intermediates; and mixed pathways $\mathbf{P_{IO}}$ and $\mathbf{P_{OI}}$. In the applied labelling the first I/O subscript denotes inner- or outer-sphere pathway for CO insertion step, while the second subscript denotes an inner- or outer-sphere pathway for ketene-imine coupling (see Scheme 7 and Scheme S1 in the ESI†).

The catalytically active Rh-PNN species may be present either in their neutral N*H*-deprotonated amido form, or in their cationic non-deprotonated amine form. Both possibilities were investigated. The pathways and species involving cationic Rh-complexes with neutral PNN*H* amine ligands are denoted with an *NH* label ($^{\mathbf{NH}}\mathbf{P}$ pathway), while the pathways and species involving neutral amido complexes with anionic (N-deprotonated) PNN^- ligands are labelled with an N label ($^{\mathbf{N}}\mathbf{P}$ pathway), see Scheme 7. A truncated ligand model of the Rh(CO)(PNN) complexes was used in all cases to limit computational costs, with all the substituents at nitrogen and phosphorus being replaced by methyl groups. Methyl diazo acetate (MDA) was used as the model diazo-compound.

Metallocarbene generation from decomposition of the diazo species starts with coordination of MDA to the square planar Rh(CO)(PNN) complex at the apical position (**INT0** → **INT1**). This step is endergonic for both the cationic species and the neutral species, but formation of the MDA adduct of the cationic amine complex is less endergonic (by −7.7 kcal mol^{-1}) than for the neutral amido complex. In contrast, and somewhat unexpectedly, subsequent N_2 elimination from the MDA adducts to give the five-coordinated metallocarbene species **INT2** has a lower barrier ($\Delta G^{\ddagger}$ = +21.7 kcal mol^{-1}) for the neutral amido complex as compared to the cationic amine complex ($\Delta G^{\ddagger}$ = +29.0 kcal mol^{-1}), despite the weaker Rh-MDA interaction in the precursor complex (transition states **TS1-2**; see Scheme 7). The lower activation barrier for rhodium-carbenoid formation at the neutral amido complex is presumably due to the more electron-rich nature of the metal centre of the neutral complex relative to the cationic amine complex, which stabilizes the carbene complex due to enhanced metal-to-carbene π-back donation. Overall, the computed diazo-activation steps to form the carbene intermediates **INT2** are similar to those proposed by Pirrung, Hengge, Wu and co-workers on the basis of experimental kinetic studies,[32] and several computational studies on other systems have revealed similar transition states for transition metal carbenoid formation from diazo compounds.[33]

Several subsequent steps were considered in the DFT calculations that provide pathways to β-lactam formation, of which several have lower total barriers than **TS1-2** (see Scheme 7 and descriptions below), implying that diazo activation must be the overall rate limiting step of the catalytic cycle. The lower barrier for rhodium-carbenoid formation at the neutral amido species is in agreement with the experimental studies, showing that the use of basic conditions (either by using K_2CO_3 or using basic tosyl hydrazone salts as substrates) is beneficial.

Two isomeric forms of the carbene species **INT2** differing in the position of the carbene ligand (in basal (*b*) and apical (*a*) positions) were considered (Fig. 2). For both the neutral amido and the cationic amine species, the carbene species $\mathbf{INT2^b}$ having the carbene in the basal position are significantlly more stable than the carbene species $\mathbf{INT2^a}$ having the carbene moiety in the apical position. Subsequent steps are considered to proceed from the lowest energy intermediate $\mathbf{INT2^b}$.

Ketene formation: inner-sphere *versus* outer-sphere CO insertion. Once the metallocarbene intermediate **INT2** is formed, several divergent reaction pathways become possible. Ketene formation can proceed by internal or external attack of CO at the carbenoid carbon atom, producing ketene adduct **INT3** or **INT6**, respectively. The outer-sphere reaction pathways have slightly lower barriers for both the cationic amine com-

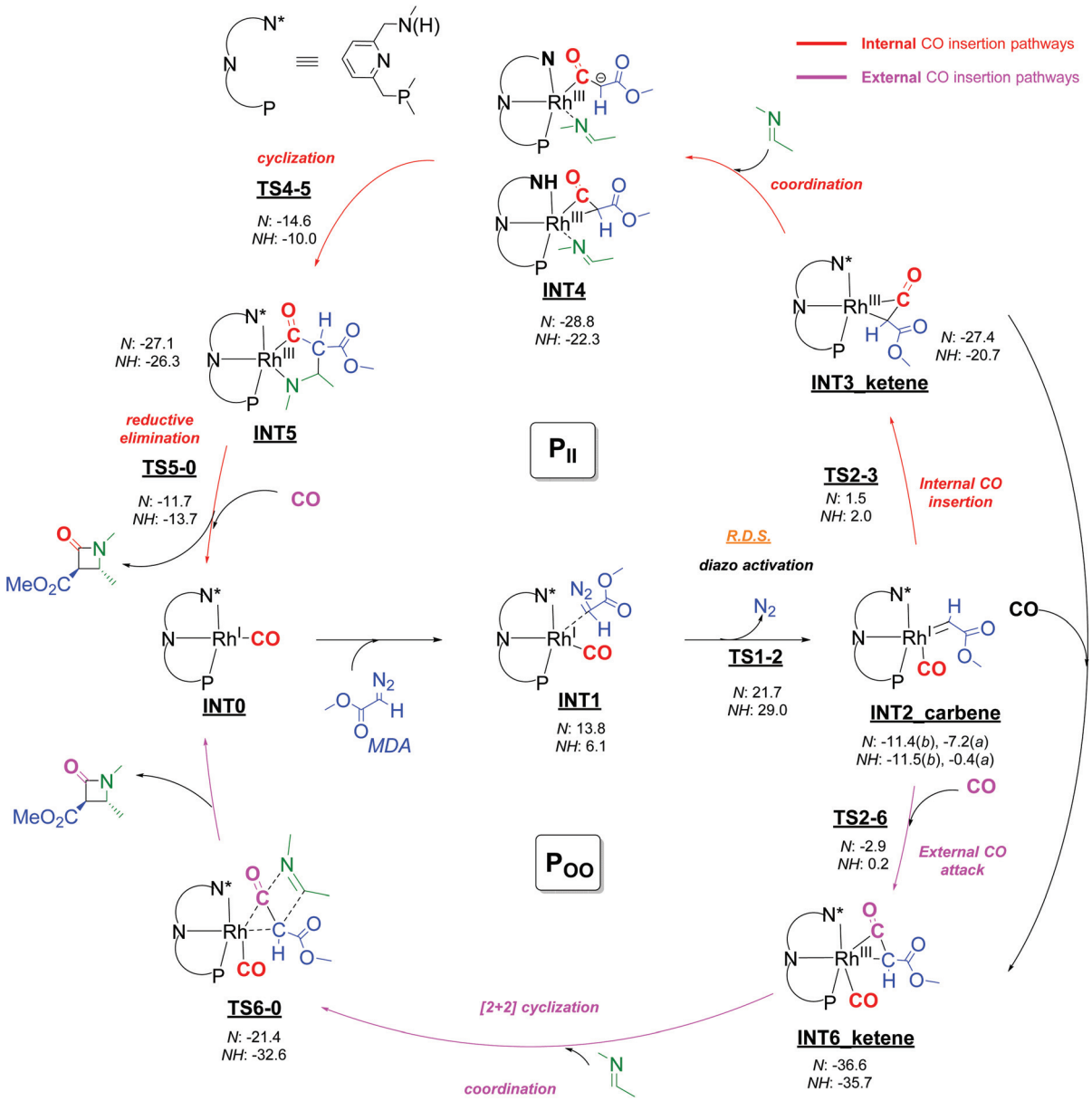

Scheme 7 DFT calculated (DFT-D3, BP86, def2-TZVP) pathways for β-lactam formation *via* catalytic generation of ketenes from rhodium-carbenoids (isodesmic, balanced reactions). Free energies (ΔG°_{298K}) in kcal mol^{-1}. All energies (also those of the transition states) are reported relative to species **INT0**. **N* and *NH* denote the amido and amino forms, respectively, of the intermediates. The metal complexes are correspondingly neutral and cationic, the labels were omitted for clarity. *For **INT2**, '*b*' indicates the carbene moiety is in a basal position; '*a*' indicates the carbene moiety is in the axial position.

plexes as well as for the neutral amido species. However, the barriers for these competing pathways are very similar.

Since the applied empirical dispersion corrections might be somewhat overestimated[34] and at the same time the computed entropy effect of the two processes are widely different with one process being intramolecular and the other being intermolecular (for which computed entropy factors are overestimated), any reliable distinction between these inner-sphere and outer-sphere pathways can probably not be made on the basis of DFT. Therefore both inner- and outer-sphere pathways for formation of the (coordinated) ketene can be considered viable, and hence both computed pathways are discussed below.

Inner-sphere ketene formation. The barriers for internal attack of CO to form the ketene species **INT3** (structure of ^{N}**INT3** shown in Fig. 3) was calculated to be +12.9 and +13.5 kcal mol^{-1} for the amido and the amino form, respectively. The **INT3** intermediates were calculated to be more stable

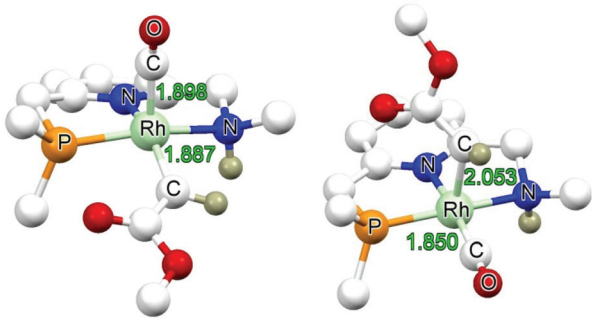

Fig. 2 DFT optimized structure of, left: ^{NH}INT2^{b}, right: ^{NH}INT2^{a} (bond lengths in Å).

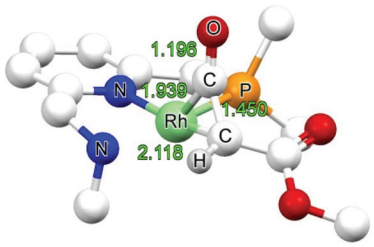

Fig. 3 DFT optimized structure of ^{N}INT3 (bond lengths in Å).

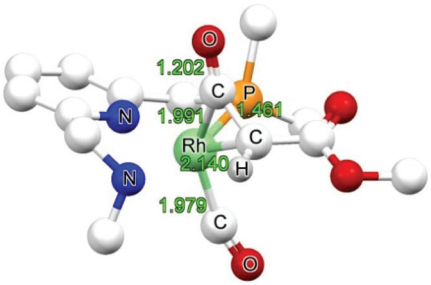

Fig. 4 DFT optimized structure of ^{N}INT6 (bond lengths in Å).

when adopting a Rh-η^2-CC_{ketene} coordination mode rather than η^2-CO_{ketene} or κ^1-O_{ketene} modes (+3.9 and +34.1 kcal mol^{-1} higher for the amido and +4.9 and +21.4 kcal mol^{-1} higher for the amine species, respectively), see Fig. 3. The ketene deviates from the coordination plane, with the C_β trans to the pyridine (for the amido **INT3**, $\angle N_{Py}$–Rh–C_β = 166.0°, $\angle N_{Py}$–Rh–C_α = 126.9°). The bonding situation is best described as a rhoda-aza-cyclopropane structure with a formal Rh^{III} oxidation state, indicated by the bond lengths in the metallacyclic fragment (for example, C_α–C_β bond lengths are 1.450 and 1.432 Å for the amido and amine form, respectively, showing single bond character). The coordination preference for η^2-CC_{ketene} over η^2-CO_{ketene} fashion is expected according to the HSAB theory,[35] as the ketene C=C moiety is "softer" than the C=O unit.[36] The amido ketene species is 6.7 kcal mol^{-1} more stable than the amine derivative, in agreement with enhanced metal-to-ligand back-donation in the former.

Outer-sphere ketene formation. External attack of CO to **INT2** leads to formation of ketene adduct **INT6.** This species is quite similar to ketene adduct **INT3**, but contains an additional carbonyl ligand. The rhodium centre in **INT6** was calculated to adopt a distorted trigonal bipyramidal coordination geometry (structure of ^{N}**INT6** shown in Fig. 4), with CO, the pyridine and the ketene occupying the equatorial positions. The metal is best described as a rhodium(III) centre in a rhoda-aza-cyclopropane structure, similar to that in **INT3**. In **TS2-6**, the external CO molecule approaches the Rh-carbene fragment, and interacts with Rh to form a distorted 6-coordinate 20e-like transition state geometry. However, **TS2-6** does not produce a stable 20e bis-carbonyl carbene intermediate (all attempts to optimize the geometry of such species either produced **INT6** by CO insertion into the carbene moiety or **INT2** by CO dissociation). Due to a weak interaction between the incoming CO molecule and the carbene moiety in **TS2-6**, the transition state directly produces **INT6** by concerted insertion of the incoming CO molecule into the Rh-carbene moiety (as confirmed by following the IRC).

Two other isomeric forms were calculated to be slightly higher in energy, one being the Rh-η^2-*CO*$_{ketene}$ isomer (+0.4 kcal mol^{-1} for the amido form) and the other having the CO coordinated *trans* to the pyridine and the ketene loosely bound at the axial position (+3.4 kcal for the amido form), suggesting possible ketene slippage and partial dissociation from the metal.

External attack of CO to **INT2** to form ketene adduct **INT6** is a process with a somewhat lower barrier (+8.5 and +11.7 kcal mol^{-1} for the amido and the amine forms, respectively) than the inner-sphere pathway to form **INT3.** Regarding the overestimation of the entropy penalty, these barriers may in reality be even lower. On the other hand the empirical dispersion effects in the approach of the CO ligand may be overestimated, and considering the rather small relative energy differences concerning these barriers, this makes it rather difficult to judge if the route *via* **TS2-3** or *via* **TS2-6** is the preferred pathway. Hence, we consider both pathways viable.

Relevance of ketene intermediates INT3 and INT6. The outer-sphere pathway leading to **INT6** is clearly more exothermic than the inner-sphere reaction producing **INT3.** In addition, formation of intermediate **INT6** by simple coordination of an additional carbonyl ligand to **INT3** is likely to occur under the applied experimental reaction conditions (CO pressure). Hence, formation of **INT6** is expected, both for the inner-sphere and for the outer-sphere pathways, and the equilibrium between these two species should lay strongly on the side of **INT6.** In that perspective, follow-up reactivity with the imine substrate could perhaps be expected to proceed preferably from the lower energy ketene intermediate **INT6** rather than from **INT3.** Nonetheless, we also considered the pathways from **INT3** relevant for β-lactam formation, as this intermediate is

less "saturated" and gives access to other substrate adducts and hence different pathway with potentially lower barriers.

Follow-up reactivity of the ketene intermediates INT3 and INT6 with the imine substrate

One possible pathway leading to β-lactam formation after formation of the ketene adducts **INT3** and **INT6** is ketene dissociation followed by an uncatalysed coupling step between the free, uncoordinated ketene and the imine substrate. However, according to DFT the uncatalysed coupling of the free (uncoordinated) ketene and imine substrates (see Scheme 8) is associated with a very high barrier of 39.7 kcal mol^{-1}.[37,38] Importantly, the computed Rh-catalysed imine-ketene coupling steps in pathways $\mathbf{P_{II}}$ and $\mathbf{P_{OO}}$ discussed below have much lower barriers (all computations performed using the same level of theory: DFT-D3, BP86, def2-TZVP), strongly suggesting that the final imine-ketene coupling steps of the β-lactam formation reaction are also Rh-catalysed.

From the neutral and cationic ketene intermediates **INT3** and **INT6** the possible pathways for Rh-catalysed β-lactam formation further diverge, and four different routes (partly interconnected by possible CO coordination/dissociation steps) were considered relevant for the formal imine [2 + 2] cyclization with the metal-bound ketene: The $\mathbf{P_{II}}$ and $\mathbf{P_{IO}}$ pathways each proceed from ketene intermediate **INT3** and concern inner-sphere and outer-sphere pathways for coupling of the imine reagent with the coordinated ketene ligand, respectively. In the pathways $\mathbf{P_{II}}$ the imine first coordinates to the metal before it couples to the ketene C=C bond, whereas in the $\mathbf{P_{IO}}$ pathway the imine directly attacks the coordinated ketene ligand as an external nucleophile. The $\mathbf{P_{OO}}$ and $\mathbf{P_{OI}}$ pathways each proceed from ketene intermediate **INT6**, and describe similar inner-sphere and outer-sphere pathways for coupling of the imine with the ketene ligand of **INT6**. These latter pathways are thus influenced by the presence of an additional CO ligand bound to rhodium. A short description of the two more plausible pathways $\mathbf{P_{II}}$ and $\mathbf{P_{OO}}$ follows below, while the alternative, but energetically less favourable pathways $\mathbf{P_{IO}}$ and $\mathbf{P_{OI}}$ are shown and discussed in some detail in the ESI (Scheme S1†).

Pathway $\mathbf{P_{II}}$: Coordination of the imine substrate to **INT3** is slightly exergonic for both the cationic amine complex and the neutral amido species, producing intermediates **INT4**. For the neutral amido form of the imine-coordinated intermediate **INT4** the ketene coordinates as an acetyl ligand with a κ^1-C_α coordination pattern, while in the cationic amine form of **INT4** the Rh-η^2-CC_{ketene}-coordination mode is maintained. Intramolecular ring-closure *via* **TS4-5** involving C–C bond formation converts **INT4** into the five-membered metallocyclic intermediates **INT5**, which produce the β-lactam product after successive reductive cyclization (**TS5-0**). For both the cationic amine and the neutral amido species, the **TS4-5** (*N*: +14.2 kcal mol^{-1}; *NH*: +12.3 kcal mol^{-1}) and **TS5-0** (*N*: +15.4 kcal mol^{-1}; *NH*: +12.6 kcal mol^{-1}) free energy barriers are very accessible, but the barriers for the cationic amine species are slightly lower than those of the neutral amido derivatives. In both cases the barriers for this pathway are much lower than the total barrier of the rate limiting diazo activation step (*N*: +21.7 kcal mol^{-1}; *NH*: +29.0 kcal mol^{-1}). Release of the product and association of CO regenerates the starting complex **INT0**, thus closing the catalytic cycle.

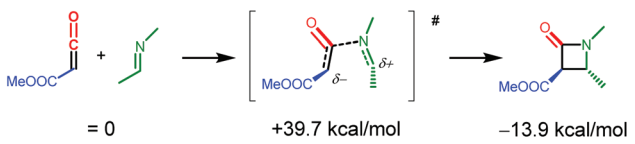

Scheme 8 DFT computed (DFT-D3, BP86, def2-TZVP) uncatalysed coupling of the free (uncoordinated) ketene and imine substrates.

Pathway $\mathbf{P_{OO}}$: The outer-sphere ketene-imine cyclization was calculated to occur in a concerted [2 + 2] step, directly at the coordinated ketene moiety of **INT6** contrasting all other pathways involving stepwise couplings. This concerted reaction step (**INT6** → **TS6-0** → **INT0** + β-lactam) directly produces the β-lactam product with regeneration of the starting complex **INT0**. It has a very low barrier for the cationic amine species ($\Delta G^{\ddagger}$ = +3.1 kcal mol^{-1}), while it has a significant but nonetheless very accessible barrier for the neutral amido species ($\Delta G^{\ddagger}$ = 15.2 kcal mol^{-1}). Considering that the rate limiting diazo activation step *via* **TS1-2** has a lower barrier for the deprotonated form of the catalyst, the barrier for the neutral amido species seems however most relevant in this $\mathbf{P_{OO}}$ pathway. This reaction pathway is a viable route for catalytic β-lactam product formation, especially considering the relative stability of intermediate **INT6** as compared to **INT3**.

Pathway $\mathbf{P_{IO}}$ and $\mathbf{P_{OI}}$: Two alternative pathways $\mathbf{P_{IO}}$ and $\mathbf{P_{OI}}$ were explored (see Scheme S1 in the ESI†), but both proceed *via* much higher barriers than pathways $\mathbf{P_{II}}$ and $\mathbf{P_{OO}}$. Pathway $\mathbf{P_{IO}}$ proceeds *via* direct attack of the imine nitrogen atom at the ketene moiety of **INT3** followed by stepwise ring closing process, with exceedingly high overall barriers from **INT3** (*N*: **INT3** → **TS8-0**, $\Delta G^{\ddagger}$ = +40.8 kcal mol^{-1}; *NH*: **INT6** → **TS8-0**, $\Delta G^{\ddagger}$ = +32.6 kcal mol^{-1}), making this route much less favourable than pathway $\mathbf{P_{II}}$. For pathway $\mathbf{P_{OI}}$, the first transition state for stepwise ring closing process represents rather high overall barriers from intermediate **INT6** (**INT6** → **TS9-10**: *N*: $\Delta G^{\ddagger}$ = +25.3 kcal mol^{-1}; *NH*: $\Delta G^{\ddagger}$ = +19.6 kcal mol^{-1}), which is clearly less favorable than pathway $\mathbf{P_{OO}}$. For more details about pathway $\mathbf{P_{IO}}$ and $\mathbf{P_{OI}}$, see the ESI.†

Brief summary of the DFT calculations

The combined DFT calculations can be summarized as follows: The activation of the diazo compound to form the carbene intermediate **INT2** appears to be the rate-limiting step of the reaction, and this step is faster upon amine deprotonation of the PNN ligand of the catalyst. Hence (in agreement with the experimental observations), it seems that the reactions preferably take place with the catalyst in its amine deprotonated form. As such, in the remaining discussion below the

energetic barriers listed are limited to those concerning the most relevant neutral amido species.

From **INT2**, the saturated and unsaturated ketene intermediates **INT6** and **INT3** can be formed, with **INT6** calculated to be lower in energy. From **INT3** pathway $\mathbf{P_{II}}$ is the lowest barrier route to β-lactam formation, while for **INT6** the lowest barrier route is the $\mathbf{P_{OO}}$ pathway ($\Delta G^{\ddagger}$ = +15.2 kcal mol^{-1}). Considering the higher stability of **INT6**, the overall barriers along the $\mathbf{P_{II}}$ pathway are somewhat higher than along the $\mathbf{P_{OO}}$ pathway ($\Delta G^{\ddagger}$ = +22.0 kcal mol^{-1} *versus* +15.2 kcal mol^{-1}). However, overestimated dispersion corrections could play a role in favoring the $\mathbf{P_{OO}}$ pathway over the $\mathbf{P_{II}}$ pathway, and hence both pathways remain viable routes to β-lactam formation. The $\mathbf{P_{IO}}$ and $\mathbf{P_{OI}}$ pathways can be safely excluded based on their relatively overall energy barriers as compared to the $\mathbf{P_{II}}$ and $\mathbf{P_{OO}}$ pathways, respectively (see Scheme S1†).

Stoichiometric experimental studies aimed at showing formation of ketenes by internal CO attack

In order to get experimental information for ketene formation, we first investigated the possibility for internal CO migration to the Rh-carbenoid moiety to form the ketene product. When two equivalents of EDA (**1**) were added to a CD_2Cl_2 solution of complex **B** at room temperature, no reaction except for dimerization of the diazo-evolved carbenoid was observed in an overnight experiment (two isomers of diethyl fumarate giving two sharp singlets at 6.2 and 6.8 ppm, respectively, see ESI, Fig. S2†). When two equivalents of *N*-tosyl hydrazone salt **5** were added to complex **B** in C_6D_6, complex **B** was immediately deprotonated, accompanied with a colour change from yellow to purple-red. Heating the solution to 55 °C for 1 hour did not produce any phenylketene. In another reaction, one equivalent of DBU was added to deprotonate the N*H* moiety of the PNN ligand of complex **B** prior to the addition of the *N*-tosyl hydrazone salt **5**, to avoid generation of the organic *N*-tosyl hydrazone precursor, which would interfere in the ^{1}H NMR spectrum. Heating the reaction mixture to 55 °C for five hours gave rise to a singlet at 4.88 ppm in the ^{1}H NMR spectrum (see ESI, Fig. S4 and S5†), which indeed indicates formation of the ketene species. Other signals are slightly broadened and hence not clear. In the ^{31}P NMR spectrum, one doublet at 49.85 ppm with a small J_{RhP} coupling constant of 137.8 Hz suggested that the PNN ligand is probably in the amido form.[39] This result indicates that inner-sphere CO insertion is indeed a viable possibility under the applied reaction conditions to form the ketene fragment, but whether or not this process is truly involved in the catalytic routes is less clear.

Conclusions

In summary, we have synthesized a series of rhodium complexes featuring new secondary amine containing PNN ligands. Complex **B** and **E** showed good activity in catalytic ketene synthesis involving carbonylation of carbenes. Amides and β-lactams can be synthesized in one-pot reactions proceeding *via in situ* generated ketene intermediates. A ketene imine has also been synthesized in a catalytic manner by reaction of a carbenoid with an isocyanide.

DFT computational studies suggest that activation of the diazo compound to generate the rhodium-carbenoid intermediate is the rate-determining step of the catalytic reaction, with the neutral amido complex being more reactive than the cationic amine complex. This is in agreement with the experimental studies, showing that the use of basic conditions (either by using K_2CO_3 or using basic tosyl hydrazone salts as substrates) is beneficial. Outer-sphere CO insertion is computed to be slightly favoured over the inner-sphere mechanism. Preliminary experimental studies show that inner sphere CO insertion to form ketene is also possible, but whether or not this process is truly involved in the catalytic routes is less clear. Additional spectrometric and kinetic studies are needed to unveil further details about the mechanism of these reactions. Follow-up coupling mechanisms most likely proceed *via* either the $\mathbf{P_{OO}}$ or $\mathbf{P_{II}}$ pathways depicted in Scheme 7, with the $\mathbf{P_{OO}}$ pathway being slightly favoured over the $\mathbf{P_{II}}$ pathway according to DFT.

Experimental details

General methods

All reactions were carried out under an argon atmosphere using standard Schlenk techniques or in a glovebox unless noted otherwise. With exception of the compounds given below, all reagents were purchased from commercial suppliers and used without further purification. *N*-Methyl-1-(6-methylpyridin-2-yl)methanamine (for synthesis of **a**)[40] and *N*-((6-methylpyridin-2-yl)methyl)aniline (for synthesis of **b**)[41] were synthesized from 6-methylpicolinaldehyde according to literature procedures. 2-(Chloromethyl)-6-((di-*tert*-butylphosphino)methyl)pyridine·BH_3 (for the synthesis of **d**) and 2-(chloromethyl)-6-((diisopropylphosphino)methyl)pyridine·BH_3 (for the synthesis of **c** and **e**) were synthesized from 2,6-bis(chloromethyl)pyridine according to a reported procedure.[42] Complex **D** was synthesized according to a reported literature procedure.[22] THF, dioxane, pentane, and diethyl ether were distilled from sodium (benzophenone as indicator) under nitrogen. CH_2Cl_2 and methanol were distilled from CaH_2 under nitrogen. *N*-Tosylhydrazone sodium salts were synthesized according to published procedures.[43,44] 6-Methylpicolinaldehyde and 2,6-bis(chloromethyl)pyridine were purchased from TCI Europe. Picolinaldehyde and ethyl diazoacetate (EDA) were purchased from Aldrich (up to 15% dichloromethane, actual content determined by NMR). NMR spectra (^{1}H, ^{31}P{^{1}H} and ^{13}C{^{1}H}) were measured on a Bruker AMX 400 spectrometer at 25 °C, unless noted otherwise. IR spectra were recorded on a Nicolet Nexus FT-IR spectrometer. HR-MS were obtained using a time-of-flight JEOL AccuTOF LC-plus mass spectrometer (JMS-T100LP).

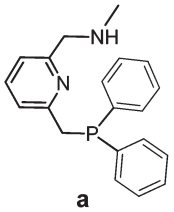

a

Ligand a. *N*-Methyl-1-(6-methylpyridin-2-yl)methanamine (680.0 mg, 4.99 mmol) was dissolved in diethyl ether (Et_2O; 30 mL) and cooled to −78 °C. *n*BuLi (1.6 M in hexane, 6.30 mL, 10.08 mmol) was slowly added, dropwise under stirring. The reaction was stirred at −78 °C for 30 minutes and subsequently allowed to warm-up slowly to 0 °C, at which temperature the mixture was stirred for 3 hours. In parallel, chlorodiphenylphosphine (1.79 mL, 9.99 mmol) was dissolved in Et_2O (30 mL) and was cooled to −78 °C. The former reaction mixture was cooled again to −78 °C and cannulated slowly to the latter solution. The reaction mixture was allowed to warm-up slowly to room temperature and stirred overnight. To quench the reaction, a 1 M HCl solution (40 mL; degassed) was added and the reaction mixture was stirred for 2 hours. Sodium carbonate (Na_2CO_3) was added slowly until a pH of approx. 8. The aqueous solution was extracted with Et_2O (3 × 40 mL). The Et_2O extracts were combined and dried over Na_2SO_4. The solid was filtered off and the Et_2O solvent removed *in vacuo*. A light-yellow oily product was obtained after purification by column chromatography under argon (eluents: hexane, then DCM). Yield: 267.0 mg (16.7%). **^{1}H NMR** (400 MHz, C_6D_6, ppm): δ 7.52–7.44 (m, $4H_{Ph}$), 7.10–7.02 (m, $6H_{Ph}$), 6.98 (td, J = 7.7, 2.5 Hz, $1H_{py}$), 6.83 (d, J = 7.1 Hz, $1H_{py}$), 6.69 (d, J = 7.7 Hz, $1H_{Py}$), 3.71 (s, $2H_{Py-CH_2N}$), 3.60 (d, J = 2.1 Hz, $2H_{Py-CH_2N}$). **^{31}P{^{1}H} NMR** (161 MHz, C_6D_6, ppm): δ −10.84 (s). **^{13}C{^{1}H} NMR** (100 MHz, C_6D_6, ppm): δ 160.07 (s, C_{Py}), 158.03 (d, J = 7.9 Hz, C_{Py}), 139.49 (s, $C_{quat\text{-}Ph}$), 139.33 (s, $C_{quat\text{-}Ph}$), 136.24 (s, C_{Py}), 133.42 (d, J = 19.1 Hz, $2C_{Ph}$), 128.73 (s, C_{Ph}), 128.60 (d, J = 6.5 Hz, $2C_{Ph}$), 121.64 (d, J = 6.1 Hz, C_{Py}), 119.42 (d, J = 2.3 Hz, C_{Py}), 57.38 (s, Py*C*H_2N), 39.06 (d, J = 17.3 Hz, Py*C*H_2P), 36.09 (s, *C*H_3). **HRMS** (ESI, 243 K, DCM): *m*/*z* 641.2975 (2M + H^+, Calcd *m*/*z* 641.2957). Ligand **a** was detected as a (H-bonded) dimer $(M)_2H^+$.

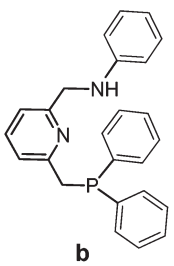

b

Ligand b. A similar procedure as used for the synthesis of ligand **a** was followed, starting from *N*-((6-methylpyridin-2-yl)-methyl)aniline (641.0 mg, 3.23 mmol). Ligand **b** was obtained as light-yellow sticky oil. Yield: 243.6 mg (19.7%). **^{1}H NMR** (400 MHz, C_6D_6, ppm): δ 7.47 (td, J = 7.3, 1.8 Hz, $4H_{Ph}$), 7.19–7.13 (m, $2H_{Ph}$), 6.90 (t, J = 7.7 Hz, $1H_{Ph}$), 6.76 (tt, J = 7.5, 1.2 Hz, $1H_{py}$), 6.67 (d, J = 7.6 Hz, $1H_{Py}$), 6.60 (d, J = 7.9 Hz, $1H_{Py}$), 6.60 (d, J = 7.9 Hz, $1H_{Py}$), 6.54–6.50 (m, $2H_{Ph}$), 4.46 (*br* s, $1H_{NH}$), 4.10 (d, J = 4.7 Hz, $2H_{Py-CH_2P}$), 3.59 (s, $2H_{Py-CH_2N}$). **^{31}P{^{1}H} NMR** (161 MHz, C_6D_6, ppm): δ −11.02 (s).

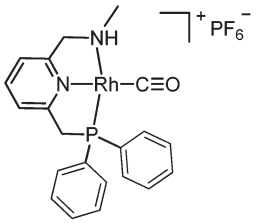

A

Complex A. A solution of ligand **a** (76.5 mg, 0.240 mmol) in methanol (2 mL) was added to a solution of $[Rh(CO)_2(\mu\text{-}Cl)]_2$ (46.6 mg, 0.120 mmol) in methanol (3 mL), followed by addition of NH_4PF_6 (78.2 mg, 0.480 mmol). The solution was stirred for one hour and the solution was concentrated to ±3 mL under vacuum. The brownish-yellow precipitate was collected by filtration and washed with a small amount of cold methanol and dried *in vacuo.* Complex **A** was obtained as a crystalline material by storing a concentrated MeOH/H_2O solution of **A** at 0 °C. Yield: 103.2 mg (72.1%). **^{1}H NMR** (400 MHz, CD_2Cl_2, ppm): δ 7.92 (td, J = 7.9; 1.1 Hz, $1H_{py4}$), 7.74–7.66 (m, $3H_{Ph}$ + $1H_{py3}$), 7.60–7.48 (m, $7H_{Ph}$), 7.44 (d, J = 7.9 Hz, $1H_{py5}$), 4.79 (dd, J = 16.5; 2.4 Hz, $2H_{Py-CH_2P}$), 4.39–4.24 (m, $2H_{Py-CH_2N}$), 4.32 (s, $1H_{NH}$), 3.09 (br s, $3H_{Me}$); **^{1}H NMR** (400 MHz, MeOD-d_4, ppm): δ 8.00 (t, J = 7.9 Hz, $1H_{py4}$), 7.82–7.71 (m, $3H_{Ph}$ + $1H_{py3}$), 7.66 (d, J = 8.1 Hz, $1H_{py5}$), 7.61–7.49 (m, $7H_{Ph}$), 6.25 (bm, $1H_{NH}$), 4.71 (dd, J = 16.7; 5.8 Hz, $1H_{Py-CHHN}$), 4.53 (dd, J = 11.7; 7.1 Hz, $2H_{Py-CH_2P}$), 4.39 (dd, 16.8, 6.5 Hz, $1H_{Py-CHHN}$), 3.02 (m, $3H_{Me}$). **^{31}P{^{1}H} NMR** (161 MHz, CD_2Cl_2, ppm): δ 52.87 (d, $^1J_{Rh-P}$ = 152.3 Hz, major), 52.66 (d, $^1J_{Rh-P}$ = 152.6 Hz, minor); **^{31}P{^{1}H} NMR** (161 MHz, MeOD-d_4, ppm): δ 52.55 (d, $^1J_{Rh-P}$ = 150.2 Hz). **^{13}C{^{1}H} NMR** (100 MHz, MeOD-d_4, ppm): δ 192.22 (dd, J = 73.4; 18.0 Hz, *C*O), 163.85 (d, J = 2.1 Hz, C_{Py2}), 161.94 (d, J = 3.1 Hz, C_{Py6}), 161.86 (s, $C_{quat\text{-}Ph}$), 142.00 (s, C_{Py4}), 133.76 (ddd, J = 12.5; 7.3; 0.9 Hz, C_{Py3}), 132.73 (d, J = 2.6 Hz, $2C_{Ph}$), 130.38 (d, J = 2.7 Hz, C_{Ph}), 130.27 (d, J = 2.6 Hz, C_{Ph}), 123.25 (d, J = 12.7 Hz, C_{Py5}), 121.13 (s, C_{Ph}), 62.99 (d, J = 2.1 Hz, Py*C*H_2N), 45.24 (d, J = 30.9 Hz, Py*C*H_2P), 43.18 (s, *C*H_3). **IR** (CD_2Cl_2, cm^{-1}): ν_{CO} 2002.5 cm^{-1}. **HRMS** (ESI, 243 K, DCM): *m*/*z* 451.0435 (M^+, Calcd *m*/*z* 451.0441).

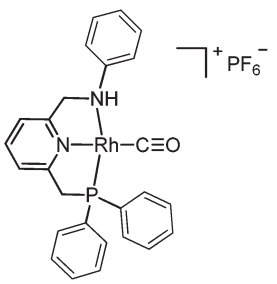

B

Complex B. A similar procedure as used for the synthesis of complex **A** was followed, but using ligand **b** (230.0 mg, 0.601 mmol) instead of ligand **a**. Complex **B** was obtained as a light yellow powder. Complex **B** was obtained as a crystalline material by top-layering a concentrated DCM solution of **B** with Et_2O. Yield: 270.2 mg (68.3%). **^{1}H NMR** (400 MHz, CD_2Cl_2, ppm): δ 7.97 (td, J = 7.9; 1.1 Hz, $1H_{py4}$), 7.75–7.63 (m, $3H_{Ph}$ + $1H_{py3}$), 7.60–7.46 (d, J = 7.9 Hz, $7H_{Ph}$ + $1H_{py5}$), 7.44–7.39 (m, $2H_{Ph}$), 7.37–7.33 (m, $2H_{Ph}$), 7.28–7.23 (m, $1H_{Ph}$) 6.71 (br d, J = 5.5 Hz, $1H_{NH}$), 5.16 (dd, J = 16.9; 6.2 Hz, $1H_{Py-CHHN}$), 4.83 (dd, J = 16.9; 5.8 Hz, $1H_{Py-CHHN}$), 4.36 (d, J = 11.7 Hz, $2H_{Py-CH_2P}$). **^{31}P{^{1}H} NMR** (161 MHz, CD_2Cl_2, ppm): δ 53.48 (d, $^1J_{Rh-P}$ = 160.0 Hz). **^{13}C{^{1}H} NMR** (100 MHz, CD_2Cl_2, ppm): δ 162.50 (d, J = 4.0 Hz, C_{Py}), 160.38 (s, C_{Ph}), 160.33 (d, J = 2.1 Hz, C_{Py}), 147.15 (s, C_{Ph}), 141.19 (s, C_{Py}), 132.99 (dd, J = 13.0; 2.6 Hz, C_{Py}), 132.25 (d, J = 1.8 Hz, $2C_{Ph}$), 130.29 (s, C_{Ph}), 129.70 (d, J = 10.8 Hz, C_{Py}), 126.59 (s, C_{Ph}), 120.89 (s, C_{Ph}), 120.31 (s, C_{Ph}), 62.69 (d, J = 1.5 Hz, Py*C*H_2N), 45.51 (d, J = 30.6 Hz, Py*C*H_2P); the carbon resonance signal of *C*O was not resolved. **IR** (CD_2Cl_2, cm^{-1}): ν_{CO} 2007.1 cm^{-1}. **HRMS** (ESI, 243 K, DCM): *m*/*z* 513.0581 (M^+, Calcd *m*/*z* 513.0598).

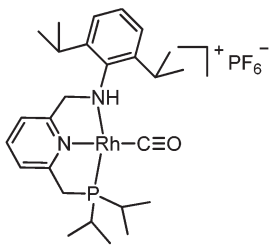

C

Complex C. A similar procedure as used for the synthesis of complex **A** was followed, but using ligand **c** (230.0 mg, 0.601 mmol) instead of ligand **a**. Complex **C** was obtained as a light-yellow powder. **^{1}H NMR** (400 MHz, CD_2Cl_2, ppm): δ 7.97 (td, J = 8.0; 0.8 Hz, $1H_{py4}$), 7.63 (d, J = 7.9 Hz, $1H_{py3}$), 7.39 (d, J = 7.9 Hz, $1H_{py5}$), 7.34–7.28 (m, $2H_{Ph3,5}$), 7.22 (dd, J = 7.0; 2.3 Hz, $1H_{Ph4}$) 6.53 (br, $1H_{NH}$), 4.87 (m, $1H_{Py-CHHN}$), 4.60 (dd, J = 17.4; 10.0 Hz, $1H_{Py-CHHN}$), 4.47 (sep, J = 6.8 Hz, $1H_{Ph-Ca H(CH_3)_2}$, *NOE correlation with NH*), 3.75 (qd, J = 18.6; 10.1 Hz, $2H_{Py-CH_2P}$), 3.23 (sep, J = 6.7 Hz, $1H_{Ph-CH(CH_3)_2}$), 2.27 (sep, J = 6.9 Hz, $2H_{PCH(CH_3)_2}$), 1.46 (d, J = 6.5 Hz, $3H_{Ph-Ca H(CH_3)_2}$), 1.44 (d, J = 6.5 Hz, $3H_{Ph-Cb H(CH_3)_2}$), 1.39 (d, J = 6.8 Hz, $3H_{Ph-Cb H(CH_3)_2}$), 1.36 (d, J = 7.2 Hz, $2H_{PCH(CH_3)_2}$), 1.33 (d, J = 6.9 Hz, $3H_{Ph-Ca H(CH_3)_2}$), 1.32 (d, J = 6.4 Hz, $2H_{PCH(CH_3)_2}$), 1.30 (d, J = 6.0 Hz, $2H_{PCH(CH_3)_2}$), 1.28–1.23 (m, $4H_{PCH(CH_3)_2}$), 1.21 (d, J = 6.9 Hz, $2H_{PCH(CH_3)_2}$). **^{31}P{^{1}H} NMR** (161 MHz, CD_2Cl_2, ppm): δ 84.79 (d, $^1J_{Rh-P}$ = 152.0 Hz). **^{13}C{^{1}H} NMR** (100 MHz, CD_2Cl_2, ppm): δ 189.93 (dd, J = 73.1; 19.1 Hz, *C*O), 161.79 (d, J = 5.2 Hz, C_{Py2}), 160.93 (s, C_{Py6}), 141.89 (s, C_{Ph1}), 141.46 (d, J = 1.4 Hz, $C_{Ph2\ or\ 6}$), 141.02 (s, C_{Py4}), 136.86 (s, $C_{Ph6\ or\ 2}$), 138.12 (s, $C_{aniline2\ or\ 6}$), 127.89 (s, $C_{Ph3\ or\ 5}$), 126.80 (s, $C_{Ph5\ or\ 3}$), 124.11 (s, C_{Ph4}), 123.02 (d, J = 11.4 Hz, C_{Py3}), 120.14 (s, C_{Py5}), 63.46 (s, Py*C*H_2N), 35.97 (d, J = 24.8 Hz, Py*C*H_2P), 29.67 (s, $PC_aH(CH_3)_2$), 28.93 (s, $PC_bH(CH_3)_2$), 26.40 (d, J = 1.9 Hz, *C*H_3), 26.40 (d, J = 1.9 Hz, PCH(*C*H_3)$_2$), 26.11 (d, J = 1.3 Hz, PCH(*C*H_3)$_2$), 25.80 (d, J = 2.1 Hz, PCH(*C*H_3)$_2$), 25.50 (d, J = 2.5 Hz, PCH(*C*H_3)$_2$), 25.49 (d, J = 8.2 Hz, P*C*H(CH$_3$)$_2$), 24.61 (s, ArCH(*C*H_3)$_2$), 23.22 (s, ArCH(*C*H_3)$_2$), 19.11 (d, J = 2.5 Hz, PCH(*C*H_3)$_2$), 18.93 (d, J = 3.4 Hz, PCH(*C*H_3)$_2$), 18.48 (s, ArCH(*C*H_3)$_2$), 17.67 (d, J = 3.4 Hz, PCH(*C*H_3)$_2$). **IR** (CD_2Cl_2, cm^{-1}) ν_{CO} 1999.1 cm^{-1}. **HRMS** (ESI, 243 K, DCM): *m*/*z* 529.1947 (M^+, Calcd *m*/*z* 529.1850).

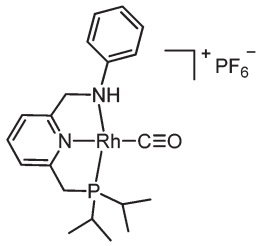

E

Complex E. A similar procedure as used for the synthesis of complex **A** was followed, but using ligand **e** (230.0 mg, 0.601 mmol) instead of ligand **a**. Complex **E** was obtained as a light yellow powder. Crystalline material of complex **E** was obtained by top-layering a concentrated DCM solution of **E** with Et_2O. **^{1}H NMR** (400 MHz, CD_2Cl_2, ppm): δ 7.92 (td, J = 7.9, 0.9 Hz, $1H_{py4}$), 7.54 (d, J = 7.9 Hz, $1H_{py3}$), 7.42 (d, J = 7.9 Hz, $1H_{py5}$), 7.39–7.34 (m, $2H_{Ph}$), 7.29–7.25 (m, $2H_{Ph}$), 7.20 (td, J = 7.2, 1.2 Hz, $1H_{Ph}$), 7.10 (bm, $1H_{NH}$), 5.12 (dd, J = 17.1, 6.3 Hz, $1H_{Py-CHHN}$), 4.71 (dd, J = 17.1, 5.1 Hz, $1H_{Py-CHHN}$), 3.65 (dd, J = 10.0, 4.2 Hz, $2H_{Py-CH_2P}$), 2.27–2.12 (m, $2H_{P-CH(CH_3)_2}$), 1.30 (d, J = 7.1 Hz, $2H_{P-CH(CH_3)_2}$), 1.22 (d, J = 7.1 Hz, $2H_{P-CH(CH_3)_2}$), 1.21 (d, J = 7.0 Hz, $2H_{P-CH(CH_3)_2}$), 1.30 (d, J = 7.1 Hz, $2H_{P-CH(CH_3)_2}$). **^{31}P{^{1}H} NMR** (161 MHz, CD_2Cl_2, ppm): δ 83.81 (d, $^1J_{Rh-P}$ = 152.8 Hz). **^{13}C{^{1}H} NMR** (100 MHz, CD_2Cl_2, ppm): δ 189.97 (dd, J = 73.2, 18.6 Hz, *C*O), 162.35 (d, J = 2.0 Hz, C_{Py2}), 161.47 (t, J = 4.2 Hz, C_{Py6}), 147.15 (d, J = 1.7 Hz, C_{Ph1}), 140.00 (s, C_{Py4}), 130.17 (s, $2C_{Ph2,6}$), 126.35 (s, C_{Ph4}), 122.58 (d, J = 11.3 Hz, C_{Py3}), 120.75 (s, $2C_{Ph3,5}$), 119.95 (s, C_{Py5}), 62.41 (d, J = 1.8 Hz, Py*C*H_2N), 35.94 (d, J = 24.5 Hz, Py*C*H_2P), 26.02 (dd, J = 29.5, 2.0 Hz, P*C*H(CH$_3$)$_2$), 18.12 (d, J = 13.6 Hz, PCH(*C*H_3)$_2$). **IR** (CD_2Cl_2, cm^{-1}) ν_{CO} 1998.6 cm^{-1}. **HRMS** (ESI, 243 K, DCM): *m*/*z* 445.0941 (M^+, Calcd *m*/*z* 445.0911).

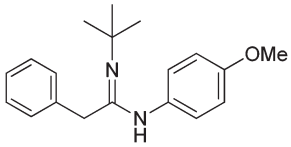

13

***N′*-(*tert*-Butyl)-*N*-(4-methoxyphenyl)-2-phenylacetimidamide (13).** **^{1}H NMR** (400 MHz, $CDCl_3$, ppm): δ 7.33–7.20 (m, 3H), 7.12 (d, J = 7.3 Hz, 2H), 6.79 (d, J = 8.6 Hz, 2H), 6.70 (d, J = 8.5 Hz, 2H), 3.87 (*b*, 1H), 3.76 (s, 3H), 3.44 (s, 2H), 1.36 (s, 9H). **^{13}C{^{1}H} NMR** (100 MHz, $CDCl_3$, ppm): δ 169.73, 154.57, 145.32, 137.20, 128.96, 128.85, 126.76, 122.73, 114.32, 55.69, 51.36, 37.60, 28.82. **MS** (EI, DCM): *m*/*z* 296 (M^+).

In situ ketene synthesis by carbene carbonylation

In a typical carbonylation experiment, a stainless steel autoclave (150 mL) suitable for seven reaction vessels (equipped with Teflon mini-stirring bars) was used to perform parallel reactions. Each vial was charged with carbene precursor (EDA **1** or *N*-tosylhydrazone sodium salt **5**, 0.15 mmol), amine nucleophile (0.30 mmol), rhodium catalyst (0.0075 mmol), internal standard 1,3,5-trimethoxybenzene (0.015 mmol) and solvent (3 mL). Before starting the catalytic reactions, the charged autoclave was purged (5×) with 20 bar of CO and then pressurized to the desired pressure. The autoclave was heated in an oil-bath with the vials being stirred overnight. After the reaction, the autoclave was cooled to 0 °C and vented to 1 atm. Around 1.5 mL was taken out of each reaction mixture, and the solvent was removed *via* rotary evaporation. The residue was dissolved in $CDCl_3$ or CH_2Cl_2 (and filtered when necessary) for ^{1}H NMR and GC-MS analysis, respectively. The conversion and yield for each reaction were calculated based on integration of the ^{1}H NMR signals of the corresponding species relative to that of the internal standard. Product assignment followed assignments presented in literature.[14e]

Ketene imine synthesis involving carbene–isocyanide coupling

A 25 mL Schlenk vessel was charged with *N*-tosylhydrazone sodium salt **5** (0.15 mmol), rhodium catalyst (0.0075 mmol), internal standard 1,3,5-trimethoxybenzene (0.015 mmol), toluene (5 mL) and *tert*-butyl isocyanide (0.75 mmol). The Schlenk vessel was then sealed and heated in an oil-bath overnight. After the reaction, around 2.5 mL was taken out of the reaction mixture, and the solvent was removed *via* rotary evaporation. The residue was dissolved in $CDCl_3$ or CH_2Cl_2 and filtered for ^{1}H NMR and GC-MS analysis, respectively. The conversion and yield for each reaction were calculated based on integration of the ^{1}H NMR signals of the corresponding species relative to that of the internal standard.

X-ray crystal structure determination of complex A

Reflections were measured on a Bruker Kappa ApexII diffractometer with sealed tube and Triumph monochromator (λ = 0.71073 Å) at a temperature of 150(2) K up to a resolution of $(\sin\theta/\lambda)_{max}$ = 0.81 Å^{-1}. The intensities were integrated with the Eval15 software.[45] Multiscan absorption correction and scaling was performed with SADABS[46] (correction range 0.67–0.75). The structure was solved with Patterson superposition methods using SHELXT.[47] Least-squares refinement was performed with SHELXL-97 [48] against F^2 of all reflections. Non-hydrogen atoms were refined freely with anisotropic displacement parameters. The coordinated amino nitrogen was disordered over two positions with a ratio 0.884(6) : 0.116(6). All hydrogen atoms were located in difference Fourier maps. The hydrogen atom at N2 was refined freely with an isotropic displacement parameter, all other H-atoms were refined with a riding model. Geometry calculations and checking for higher symmetry was performed with the PLATON program.[49]

X-ray crystal structure details of complex A

$[C_{21}H_{21}N_2OPRh](PF_6)\cdot CH_3OH$, Fw = 628.29, yellow block, 0.57 × 0.35 × 0.18 mm^3, triclinic, $P\bar{1}$ (no. 2), a = 9.70447(19), b = 9.77001(15), c = 14.1603(3) Å, α = 83.358(1), β = 74.636(1), γ = 74.636(1)°, V = 1246.84(4) Å^3, Z = 2, D_x = 1.674 g cm^{-3}, μ = 0.88 mm^{-1}. 41 801 reflections were measured up to a resolution of $(\sin\theta/\lambda)_{max}$ = 0.81 Å^{-1}. 10 952 reflections were unique (R_{int} = 0.015), of which 10 239 were observed [$I > 2\sigma(I)$]. 330 parameters were refined with 1 restraint (C–N distance of the disordered group). R_1/wR_2 [$I > 2\sigma(I)$]: 0.0221/0.0567. R_1/wR_2 [all refl.]: 0.0243/0.0577. S = 1.057. Residual electron density between −0.53 and 0.61 e Å^{-3}. CCDC 1424620.

X-ray crystal structure determination of complexes B and E

X-ray intensities were measured on a Bruker D8 Quest Eco diffractometer equipped with a Triumph monochromator (λ = 0.71073 Å) and a CMOS Photon 50 detector at a temperature of 150(2) K. Intensity data were integrated with the Bruker APEX2 software.[50] Absorption correction and scaling was performed with SADABS.[46] The structures were solved with the program SHELXL.[50] Least-squares refinement was performed with SHELXL-2013 [51] against F^2 of all reflections. Non-hydrogen atoms were refined with anisotropic displacement parameters. The H atoms were placed at calculated positions using the instructions AFIX 13, AFIX 43 or AFIX 137 with isotropic displacement parameters having values 1.2 or 1.5 times U_{eq} of the attached C atoms.

X-ray crystal structure details of complex B

$C_{26}H_{23}N_2OPRh\ PF_6$, Fw = 658.31, yellow block, 0.389 × 0.319 × 0.112 mm^3, Monoclinic, $P21/c$, a = 10.6439(13), b = 11.6245(14), c = 21.782(2) Å, β = 100.416(2)°, V = 2650.7(5) Å^3, Z = 4, D_x = 1.650 g cm^{-3}, μ = 0. 831 mm^{-1}. 30 389 reflections were measured up to a resolution of $(\sin\theta/\lambda)_{max}$ = 0.59 Å^{-1}. 4661 Reflections were unique (R_{int} = 0.0711), of which 3905 were observed [$I > 2\sigma(I)$]. 346 Parameters were refined with 334 restraints (RIGU). R_1/wR_2 [$I > 2\sigma(I)$]: 0.0382/0.0948. R_1/wR_2 [all refl.]: 0.0510/0.1062. S = 1.038. CCDC 1423805.

X-ray crystal structure details of complex E

$C_{20}H_{27}N_2OPRh\ PF_6$, Fw = 590.29, yellow-brown block, 0.886 × 0.217 × 0.126 mm^3, monoclinic, $P21/n$, a = 13.4021(9), b = 10.9937(7), c = 15.6906(10) Å, β = 97.462(3)°, V = 2292.3(3) Å^3, Z = 4, D_x = 1.710 g cm^{-3}, μ = 0. 949 mm^{-1}. 97 401 reflections were measured up to a resolution of $(\sin\theta/\lambda)_{max}$ = 0.91 Å^{-1}. 14 600 reflections were unique (R_{int} = 0.0669), of which 10 763 were observed [$I > 2\sigma(I)$]. 297 Parameters were refined with 279 restraints (RIGU). R_1/wR_2 [$I > 2\sigma(I)$]: 0.0381/0.0833. R_1/wR_2 [all refl.]: 0.0675/0.0988. S = 1.075. CCDC 1423806.

CCDC 1424620, 1423805 and 1423806 contain the supplementary crystallographic data for compound **A**, **B** and **E**, respectively.

Details of the DFT calculations

Geometry optimizations were carried out with the Turbomole program package[52] coupled to the PQS Baker optimizer[53] *via* the BOpt package,[54] at the ri-DFT level using the BP86[55] functional and the resolution-of-identity (ri) method.[56] The geometries of all stationary points were optimized at the def2-TZVP basis set level,[57] both with and without Grimme's dispersion corrections (disp3 version).[58] The identity of the transition states was confirmed by following the imaginary frequency in both directions (IRC). All minima (no imaginary frequencies) and transition states (one imaginary frequency) were characterized by calculating the Hessian matrix. ZPE and gas-phase thermal corrections (entropy and enthalpy, 298 K, 1 bar) from these analyses were calculated. The relative (free) energies obtained from these calculations are reported in Scheme 7.

Acknowledgements

This research was funded by the Netherlands Organization for Scientific Research, section Chemical Sciences (NWO-CW; ECHO grant to BdB). JIvdV thanks the ERC for a Starting Grant (279097, EuReCat). The ApexII diffractometer at Utrecht University has been financed by NWO-CW. We thank Ed Zuidinga for performing the ESI-MS measurements.

Notes and references

1 (*a*) H. Staudinger, *Ber. Dtsch. Chem. Ges.*, 1905, **38**, 1735; (*b*) T. T. Tidwell, *Eur. J. Org. Chem.*, 2006, 563; (*c*) D. H. Paull, A. Weatherwax and T. Lectka, *Tetrahedron*, 2009, **65**, 6771.

2 (*a*) A. D. Allen and T. T. Tidwell, *Eur. J. Org. Chem.*, 2012, 1081; (*b*) A. D. Allen and T. T. Tidwell, *Chem. Rev.*, 2013, **113**, 7287.

3 (*a*) H. Staudinger and J. Meyer, *Chem. Ber.*, 1920, **53**, 72; (*b*) H. Perst, in *Science of Synthesis*, ed. R. L. Danheiser, Product Class 17: Ketenimines, 781, Georg Thieme Verlag, Stuttgart, 2006, vol. 23; (*c*) S. H. Kim, S. H. Park, J. H. Choi and S. Chang, *Chem. – Asian J.*, 2011, **6**, 2618; (*d*) S. E. Denmark and T. W. Wilson, *Angew. Chem., Int. Ed.*, 2012, **51**, 9980; (*e*) P. Lu and Y. Wang, *Chem. Soc. Rev.*, 2012, **41**, 5687; (*f*) C. Fromont and S. Masson, *Tetrahedron*, 1999, **55**, 5405; (*g*) G. A. Gornowicz and R. West, *J. Am. Chem. Soc.*, 1971, **93**, 1714; (*h*) I. Bae, H. Han and S. Chang, *J. Am. Chem. Soc.*, 2005, **127**, 2038.

4 H. W. Moore and D. S. Wilbur, *J. Org. Chem.*, 1980, **45**, 4483.

5 (*a*) Y. Chiang, A. J. Kresge and V. V. Popik, *J. Am. Chem. Soc.*, 1999, **121**, 5930; (*b*) B. D. Wagner, B. R. Arnold, G. S. Brown and J. Lusztyk, *J. Am. Chem. Soc.*, 1998, **120**, 1827.

6 L. S. Hegedus, J. Montgomery, Y. Narukawa and D. C. Snustad, *J. Am. Chem. Soc.*, 1991, **113**, 5784.

7 Y. Yang, W. Shou, D. Hong and Y. Wang, *J. Org. Chem.*, 2008, **73**, 3574.

8 (*a*) G. A. Gornowicz and R. West, *J. Am. Chem. Soc.*, 1971, **93**, 1714; (*b*) M. Bendikov, H. M. Duong, E. Bolanos and F. Wudl, *Org. Lett.*, 2005, **7**, 783; (*c*) Y. Zhang, K. A. DeKorver, A. G. Lohse, Y. Zhang, J. Huang and R. P. Hsung, *Org. Lett.*, 2009, **11**, 899; (*d*) K. A. DeKorver, X. N. Wang, M. C. Walton and R. P. Hsung, *Org. Lett.*, 2012, **14**, 1768.

9 (*a*) M. P. Cassidy, J. Raushel and V. V. Fokin, *Angew. Chem., Int. Ed.*, 2006, **45**, 3154; (*b*) M. Whiting and V. V. Fokin, *Angew. Chem., Int. Ed.*, 2006, **45**, 3157.

10 (*a*) N. Ungvári and F. Ungváry, Carbonylation of diazoalkanes, in *Modern Carbonylation Methods*, ed. L. Kollár, Wiley-VCH, Weinheim, 2008, ch. 8, p. 199; (*b*) K. H. Dötz and J. Stendel, *Chem. Rev.*, 2009, **109**, 3227.

11 H. Staudinger and O. Kupfer, *Ber. Dtsch. Chem. Ges.*, 1912, **45**, 501.

12 (*a*) K. H. Dötz and J. Mühlemeier, *Angew. Chem., Int. Ed. Engl.*, 1982, **21**, 929; (*b*) P. T. Barger, B. D. Santarsiero, J. Armantrout and J. E. Bercaw, *J. Am. Chem. Soc.*, 1984, **106**, 5178–5186; (*c*) N. Ungvári, E. Fördős, J. Balogh, T. Kégl, L. Párkányi and F. Ungváry, *Organometallics*, 2010, **29**, 3837.

13 TM-catalysed carbonylation of dihalides: (*a*) A. Miyashita, T. Kihara, K. Nomura and H. Nohira, *Chem. Lett.*, 1986, 1607; (*b*) M. Huser, M. Youinou and J. A. Osborn, *Angew. Chem., Int. Ed. Engl.*, 1989, **28**, 1386.

14 TM-catalysed carbonylation of diazo compounds: (*a*) T. Ye and M. A. Mckervey, *Chem. Rev.*, 1994, **94**, 1091; (*b*) R. Tuba and F. Ungváry, *J. Mol. Catal. A: Chem.*, 2003, **203**, 59; (*c*) Z. Zhang and J. Wang, *Tetrahedron*, 2008, **64**, 6577; (*d*) E. Fördos, R. Tuba, L. Párkányl, T. Kégl and F. Ungváry, *Eur. J. Org. Chem.*, 2009, 1994; (*e*) Z. Zhang, Y. Liu, L. Ling, Y. Li, Y. Dong, M. Gong, X. Zhao, Y. Zhang and J. Wang, *J. Am. Chem. Soc.*, 2011, **133**, 4330; (*f*) N. D. Paul, A. Chirila, H. Lu, X. P. Zhang and B. de Bruin, *Chem. – Eur. J.*, 2013, **19**, 12953; (*g*) Z. Zhang, Y. Zhang and J. Wang, *ACS Catal.*, 2011, **1**, 1621; (*h*) Q. Xiao, Y. Zhang and J. Wang, *Acc. Chem. Res.*, 2013, **46**, 236.

15 J. R. Fulton, V. K. Aggarwal and J. De Vicente, *Eur. J. Org. Chem.*, 2005, 1479.

16 C. R. Pitts and T. Lectka, *Chem. Rev.*, 2014, **114**, 7930.

17 (*a*) J. A. Green and L. A. Singer, *Tetrahedron Lett.*, 1969, 5093; (*b*) T. W. Hudnall, E. J. Moorhead, D. G. Gusev and C. W. Bielawski, *J. Org. Chem.*, 2010, **75**, 2763; (*c*) G. A. Blake, J. P. Moerdyk and C. W. Bielawski, *Organometallics*, 2012, **31**, 3373; (*d*) D. Martin, Y. Canac, V. Lavallo and G. Bertrand, *J. Am. Chem. Soc.*, 2014, **136**, 5023.

18 (*a*) F. Zhou, K. Ding and Q. Cai, *Chem. – Eur. J.*, 2011, **17**, 12268; (*b*) Q. Dai, Y. Jiang, J.-T. Yu and J. Cheng, *Chem. Commun.*, 2015, DOI: 10.1039/c5cc06771e.

19 R. Lindner, B. van den Bosch, M. Lutz, J. N. H. Reek and J. I. van der Vlugt, *Organometallics*, 2011, **30**, 499.

20 (*a*) E. Fogler, J. A. Garg, P. Hu, G. Leitus, L. J. W. Shimon and D. Milstein, *Chem. – Eur. J.*, 2014, **20**, 15727.

21 C. Tejel, M. P. Río, L. Asensio, F. J. Van Den Bruele, M. A. Ciriano, N. Tsichlis i Spithas, D. G. H. Hetterscheid and B. de Bruin, *Inorg. Chem.*, 2011, **50**, 7524.

22 For complex **D**, see: Z. Tang, E. Otten, J. N. H. Reek, J. I. van der Vlugt and B. de Bruin, *Chem. – Eur. J.*, 2015, **21**, 12683–12693.

23 N2 of complex **A** is distorted over two positions with a ratio of 0.88 : 0.12, see ESI.†

24 Addition of K_2CO_3 (22.2 mg, 0.161 mmol) to a solution of **B** (27.1 mg, 0.041 mmol) in THF (1.5 mL) led to immediate color change from yellow to orange-red. The ^{31}P NMR spectrum of the reaction solution showed a doublet at 49.58 ($^1J_{RhP}$ = 141.5). The high-field chemical shift and remarkable decrease in coupling constant are indicative of N*H* deprotonation to generate a strong donor *trans* to phosphorus.

25 (*a*) J.-M. Lehn, *Chem. – Eur. J.*, 1999, **5**, 2455–2463; (*b*) M. Ciaccia and S. Di Stefano, *Org. Biomol. Chem.*, 2015, **13**, 646–654.

26 Alternatively, **7a** could be formed by direct coupling of the metallocarbene intermediate **II** and the aniline nucleophile, followed by a parallel dehydrogenation process. However, no dehydrogenation or transfer hydrogenation of benzylamine was observed when using **B′** or **E′** as the catalyst under similar conditions, indicating a fast dehydrogenation process of a metal-bound amine/amido intermediate following the undesired C–N coupling, if that is the case.

27 (*a*) R. B. Morin and M. Gorman, *Chemistry and Biology of β-Lactam Antibiotics*, Academic Press, New York, 6th edn, 1982; (*b*) B. Alcaide, P. Almendros and C. Aragoncillo, *Chem. Rev.*, 2007, **107**, 4437; (*c*) T. T. Tidwell, *Angew. Chem., Int. Ed.*, 2008, **47**, 1016; (*d*) N. A. A. El-Kanzi, *Heterocycl. Lett.*, 2013, **3**, 81; (*e*) A. Gupta and A. K. Halve, *Int. J. Pharm. Sci. Res.*, 2015, **6**, 978.

28 (*a*) M. Staudinger, *Justus Liebigs Ann. Chem.*, 1907, **356**, 51; (*b*) G. I. Georg and V. T. Ravikumar, in *The Organic Chemistry of β-Lactams*, ed. G. I. Georg, Verlag Chemie, New York, 1993, p. 295; (*c*) C. Palomo, J. M. Aizpurua, I. Ganboa and M. Oiarbide, *Curr. Med. Chem.*, 2004, **11**, 1837; (*d*) R. Tuba, *Org. Biomol. Chem.*, 2013, **11**, 5976.

29 (*a*) L. S. Hegedus, J. Montgomery, Y. Narukawa and D. C. Snustad, *J. Am. Chem. Soc.*, 1991, **113**, 5784; (*b*) S. France, A. Weatherwax, A. E. Taggi and T. Lectka, *Acc. Chem. Res.*, 2004, **37**, 592; (*c*) Y. Wang, Y. Liang, L. Jiao, D. M. Du and J. Xu, *J. Org. Chem.*, 2006, **71**, 6983; (*d*) B. K. Banik, B. Lecea, A. Arrieta, A. De Cózar and F. P. Cossío, *Angew. Chem., Int. Ed.*, 2007, **46**, 3028; (*e*) F. P. Cossío, A. Arrieta and M. A. Sierra, *Acc. Chem. Res.*, 2008, **41**, 925; (*f*) H. Qi, X. Li and J. Xu, *Org. Biomol. Chem.*, 2011, **9**, 2702.

30 R. Tuba, *Org. Biomol. Chem.*, 2013, **11**, 5976.

31 (*a*) A. Arrieta, F. P. Cossı, I. Ferna and M. J. Manchen, *J. Am. Chem. Soc.*, 2000, **122**, 11509; (*b*) I. Ferna, M. a. Sierra, J. Manchen, M. Go and F. P. Cossi, *J. Am. Chem. Soc.*, 2008, **130**, 13892.

32 (*a*) M. C. Pirrung, H. Liu and A. T. Morehead Jr., *J. Am. Chem. Soc.*, 2002, **124**, 1014; (*b*) F. M. Wong, J. Wang, A. C. Hengge and W. Wu, *Org. Lett.*, 2007, **9**, 1663.

33 (*a*) E. Nakamura, N. Yoshikai and M. Yamanaka, *J. Am. Chem. Soc.*, 2002, **124**, 7181; (*b*) J. Hansen, J. Autschbach and H. M. L. Davies, *J. Org. Chem.*, 2009, **74**, 6555; (*c*) N. D. Paul, S. Mandal, M. Otte, X. Cui, X. P. Zhang and B. de Bruin, *J. Am. Chem. Soc.*, 2014, **136**, 1090; (*d*) W. I. Dzik, X. Xu, X. P. Zhang, J. N. H. Reek and B. de Bruin, *J. Am. Chem. Soc.*, 2010, **132**, 10891; (*e*) A. J. C. Walters, J. N. H. Reek and B. de Bruin, *ACS Catal.*, 2014, **4**, 1376.

34 (*a*) T. Schwabe and S. Grimme, *Phys. Chem. Chem. Phys.*, 2007, **9**, 3397; (*b*) K. E. Riley and M. Piton, *Chem. Rev.*, 2010, **110**, 5023; (*c*) J. P. P. Ramalho, J. R. B. Gomes and F. Illas, *RSC Adv.*, 2013, **3**, 13085.

35 (*a*) R. G. Pearson, *J. Am. Chem. Soc.*, 1963, **85**, 3533; (*b*) R. G. Pearson, *Science*, 1966, **151**, 172; (*c*) R. G. Pearson, *Chemical Hardness - Applications From Molecules to Solids*, Wiley-VCH, Weinheim, 1997.

36 (*a*) H. Werner and E. Bleuel, *Angew. Chem., Int. Ed.*, 2001, **40**, 145; (*b*) D. B. Grotjahn, L. S. B. Collins, M. Wolpert, G. a. Bikzhanova, H. C. Lo, D. Combs and J. L. Hubbard, *J. Am. Chem. Soc.*, 2001, **123**, 8260.

37 The direct uncatalysed concerted (but non-synchronous) [2 + 2] cycloaddition reaction of the *trans*-imine MeC═NMe and ketene OC═CHCOOMe in the gas phase was considered, without any proton- or Lewis-acid-assistance (*i.e.* not acid-catalysed). This barrier seems most relevant for comparison with the Rh-catalysed pathways considering the fact that the experimental reactions were performed under basic reaction conditions.

38 Rather high reaction barriers were also obtained in other studies of [2 + 2] cyclo-addition reactions involving several differently substituted ketenes and imines and using various computational models: (*a*) B. K. Banik, B. Lecea, A. Arrieta, A. de Cózar and F. P. Cossío, *Angew. Chem., Int. Ed.*, 2007, **46**, 3028; (*b*) N. Fu and T. T. Tidwell, *Tetrahedron*, 2008, **64**, 10465; (*c*) C. Zhou, *Studies on cycloaddition reactions of ketenes: further investigations of pseudopericyclic reaction mechanisms*, PhD Thesis, Texas Tech University, 2004, http://hdl.handle.net/2346/10697.

39 L. S. Jongbloed, B. de Bruin, J. N. H. Reek, M. Lutz and J. I. van der Vlugt, *Chem. – Eur. J.*, 2015, **21**, 7297.

40 M. Seitz, A. Kaiser, A. Tereshchenko, C. Geiger, Y. Uematsu and O. Reiser, *Tetrahedron*, 2006, **62**, 9973.

41 G. J. P. Britovsek, J. England and A. J. P. White, *Dalton Trans.*, 2006, 1399.

42 M. Gargir, Y. Ben-David, G. Leitus, Y. Diskin-Posner, L. J. W. Shimon and D. Milstein, *Organometallics*, 2012, **31**, 6207.

43 J. R. Fulton, V. K. Aggarwal and J. de Vicente, *Eur. J. Org. Chem.*, 2005, 1479.

44 (*a*) P. Doppelt, J. Fischer and R. Webs, *Inorg. Chem.*, 1984, **23**, 2958–2962; (*b*) R. L. Halterman and S. T. Jan, *J. Org. Chem.*, 1991, **56**, 5253; (*c*) X. Xu, H. Lu, J. V. Ruppel, X. Cui,

S. L. de Mesa, L. Wojtas and X. P. Zhang, *J. Am. Chem. Soc.*, 2011, **133**, 15292.
45 A. M. M. Schreurs, X. Xian and L. M. J. Kroon-Batenburg, *J. Appl. Crystallogr.*, 2010, **43**, 70.
46 G. M. Sheldrick, *SADABS*, Universität Göttingen, Germany, 2008.
47 G. M. Sheldrick, *Acta Crystallogr., Sect. A: Fundam. Crystallogr.*, 2015, **71**, 3.
48 G. M. Sheldrick, *Acta Crystallogr., Sect. A: Fundam. Crystallogr.*, 2008, **64**, 112.
49 A. L. Spek, *Acta Crystallogr., Sect. D: Biol. Crystallogr.*, 2009, **65**, 148.
50 Bruker, *APEX2 software*, Madison WI, USA, 2014.
51 G. M. Sheldrick, *SHELXL2013*, University of Göttingen, Germany, 2013.
52 R. Ahlrichs, *Turbomole Version 6.5*, Theoretical Chemistry Group, University of Karlsruhe.
53 *PQS version 2.4*, Parallel Quantum Solutions, Fayettevile, Arkansas, USA, 2001; the Baker optimizer is available separately from PQS upon request: I. Baker, *J. Comput. Chem.*, 1986, **7**, 385.
54 P. H. M. Budzelaar, *J. Comput. Chem.*, 2007, **28**, 2226.
55 (*a*) A. D. Becke, *Phys. Rev. A*, 1988, **38**, 3098; (*b*) J. P. Perdew, *Phys. Rev. B: Condens. Matter*, 1986, **33**, 8822.
56 M. Sierka, A. Hogekamp and R. Ahlrichs, *J. Chem. Phys.*, 2003, **118**, 9136.
57 A. Schaefer, H. Horn and R. Ahlrichs, *J. Chem. Phys.*, 1992, **97**, 2571.
58 S. Grimme, J. Antony, S. Ehrlich and H. Krieg, *J. Chem. Phys.*, 2010, **132**, 154.